

2mit
NATIONAL AERONAUTICS AND SPACE ADMINISTRATION

Technical Memorandum 33-656

*Solid Motor Diagnostic
Instrumentation*

Y. Nakamura

W. E. Arens

W. S. Wuest

(NASA-CR-136561). SOLID MOTOR DIAGNOSTIC
INSTRUMENTATION (Jet Propulsion Lab.) N74-15459
83 p HC \$6.25 CSCL 21H
84
G3/28 Unclass 26760



JET PROPULSION LABORATORY
CALIFORNIA INSTITUTE OF TECHNOLOGY
PASADENA, CALIFORNIA

December 1, 1973

NATIONAL AERONAUTICS AND SPACE ADMINISTRATION

Technical Memorandum 33-656

*Solid Motor Diagnostic
Instrumentation*

Y. Nakamura

W. E. Arens

W. S. Wuest

**JET PROPULSION LABORATORY
CALIFORNIA INSTITUTE OF TECHNOLOGY
PASADENA, CALIFORNIA**

December 1, 1973

**Prepared Under Contract No. NAS 7-100
National Aeronautics and Space Administration**

PREFACE

The work described in this report was performed by the Propulsion, Astrionics, and Telecommunications Divisions of the Jet Propulsion Laboratory.

PRECEDING PAGE BLANK NOT FILMED

ACKNOWLEDGEMENT

The authors would like to acknowledge the cooperation of the many organizations, NASA, and other government agencies for their invaluable assistance during the conduct of this study. Special mention is made of M. E. Ellion, D. P. Frizell, and L. M. Spicer of Hughes Aircraft Company; A. C. Ellings and K. Nall, Systems Group of TRW, Inc.; E. M. Landsbaum of Aerospace Corporation; J. R. Trout and L. Meyer of AFRPL; J. Hulbert and K. Sater of Philco-Ford Corporation; K. W. Bills of Aerojet Solid Propulsion Company; and D. W. Dembrow of Goddard Space Flight Center. The authors would further like to acknowledge the significant contributions and assistance by L. B. Paulos, R. Dickinson, and W. L. Dowler in their areas of specialties.

CONTENTS

I. Introduction	1
II. Summary	3
III. Technical Approach	4
IV. Technology Review	5
A. Overview of Typical Failures	5
B. Existing Monitoring and Surveillance Practices	7
C. Available Instruments	10
V. SMDI Requirements	11
A. System Requirements and Objectives	11
B. Failure Modes and Effects	14
VI. Conceptual Design	16
A. Hardened CDR Design	16
B. Unhardened CDR Design	26
C. Sensors and Signal Processing	29
D. Comparison of Candidate Approaches	30
VII. Conclusions and Recommendations	31
References	33
Appendix. Typical Solid Motor Specification Requirements	71

TABLES

1. Findings of failure review board investigations	35
2. Storage and transportation data.	36
3. Representative monitoring and surveillance practices	37
4. Typical available instruments	38
5. Solid motor diagnostic instrumentation characteristics	39
6. Thresholded data system requirements	40

7.	Failure modes and effects summary for real-time system. . .	41
8.	Failure mode detection and discrimination for thresholded system	42
9.	CDR timed events.	44
10.	CDR non-timed events.	45
11.	Spacecraft radio transmission parameters — hardened design	46
12.	Radio reception parameters — hardened design	47
13.	Telemetry parameters — hardened design	48
14.	Telecommunications link design control table — hardened design	49
15.	CDR weight and volume breakdown — hardened design.	50
16.	CDR cost summary — hardened design	51
17.	Spacecraft radio transmission parameters — unhardened design	52
18.	Radio reception parameters — unhardened design.	53
19.	Telemetry parameters — unhardened design	54
20.	Telecommunications link design control table — unhardened design	55
21.	Unhardened CDR design weight and volume breakdown	56
22.	Unhardened CDR design cost summary	57
23.	Typical sensor and amplifier package	58
24.	Summary of functional and unit characteristics of candidate designs	59
25.	Summary of SMDI candidate design properties	60
A-1.	SVM-1 specification requirements	71
A-2.	SVM-2 specification requirements.	72
A-3.	TE-M-521 specification requirements	73
A-4.	TE-M-364-3 specification requirements.	74
A-5.	FW-4S specification requirements	75
A-6.	TE-364-1 specification requirements	76

FIGURES

1.	SMDI system block diagram	61
2.	Typical CDR data frame	62
3.	Oscillatory event detection circuitry	63
4.	CDR data encoder real-time data processing	64
5.	CDR subassembly integration	65
6.	CDR battery I (28 Vdc \pm 10%) current profile.	66
7.	CDR battery II (10 Vdc \pm 10%) current profile	67
8.	CDR power for real-time data mode	68
9.	Unhardened CDR design subassembly	69
10.	CDR subassembly integration — unhardened design.	70

ABSTRACT

A review of typical surveillance and monitoring practices followed during the flight phases of representative solid-propellant upper stages and apogee motors was conducted to evaluate the need for improved flight diagnostic instrumentation on future spacecraft. The findings of previous failure review boards were also reviewed and factored into the study to identify critical parameters and instrumentation requirements associated with these diagnostic traces. To bound the problem, the capabilities of the flight instrumentation package were limited to the detection of whether or not the solid motor was the cause of failure and to the identification of probable primary failure modes. Conceptual designs of self-contained flight instrumentation packages capable of meeting these requirements were generated and their performance, typical cost, and unit characteristics determined. Comparisons of a continuous real-time and a thresholded hybrid design were made on the basis of performance, mass, power, cost, and expected life. The results of this analysis substantiated the feasibility of a self-contained independent flight instrumentation module as well as the existence of performance margins by which to exploit growth option applications.

I. INTRODUCTION

Because of the total number of recent incidents in which failures during the operation of solid propellant rocket upper-stage or apogee-boost motors have occurred, a great deal of concern regarding the reliability of this class of high performance motor has been raised. Although considerable engineering data from on-board instrumentation are transmitted during both the launch and apogee motor burns, most of these data are necessarily dedicated to spacecraft performance information. Failure review board reports for these past motor failures make it clear that the transmitted information is

often far from adequate to identify which subsystem failed and the probable failure mode. Hence, a need exists to identify a simple diagnostic instrumentation module capable of providing added information in the event of a flight anomaly or failure and further insight in identifying failure modes, mechanisms, and potential solutions.

To this end, a preliminary study was initiated by the Propulsion Division of the Jet Propulsion Laboratory to evaluate the feasibility of developing a universal flight instrumentation package capable of monitoring critical solid propulsion system parameters during launch and apogee motor burns. The specific objective of this study was to identify a suitable universal instrumentation package concept, independent of the spacecraft telemetry system, capable of detecting and discriminating whether or not the solid motor was the cause of failure. A secondary objective was to identify the probable primary failure mode(s) in the event the solid motor had malfunctioned. The intent of this study was to identify a minimum-capability minimum-cost package that would yield the necessary diagnostic information while minimizing the impact upon related subsystems within the spacecraft complex. No attempt was made to provide the package with capabilities beyond diagnostic detection and discrimination.

Two candidate solutions have been offered in the form of independent diagnostic packages, each of which is capable of providing added information in the event of a flight anomaly or failure and further insight into identifying probable failure modes, mechanisms, and potential solutions.

The first approach entails the use of a hybrid (real-time/nonreal-time) system that maximizes the probability of data acquisition regardless of failure mode or spacecraft conditions. In this design performance margins have been identified by which to exploit growth options and/or further reduce cost, weight, power, and size of the basic unit.

The alternate design involves a smaller, lighter, and cheaper package that provides real-time coverage. Although this system cannot survive catastrophic failures and is frequency response limited, the resultant coverage is expected to suffice in the vast majority of cases.

A companion study evaluating system effects on motor reliability examined possible correlation between system factors and service failures

of selective apogee and upper-stage solid propellant motors (Ref. 1). In that study, an assessment of comparable instrumentation and procedures required during the ground handling and storage phases of solid rocket motors was addressed in determining whether a motor might have been damaged in storage, handling, or transportation.

The work described herein and the parallel motor reliability study represent a continuing attempt to provide spacecraft designers with added insight into identifying potential failure modes and solutions to enhance the reliability of future flight programs which will employ solid-propellant rocket motors.

II. SUMMARY

Two candidate special-purpose solid motor diagnostic instrumentation (SMDI) systems have been identified to monitor the performance of solid rocket upper stage and apogee motors. Each of the candidate designs is completely independent of the spacecraft power and radio systems (with the exception of turn-on and motor ignition signals) so that failures in those systems can be distinguished from propulsion failures. Additionally, each system emphasizes the use of state-of-the-art technology and hardware as well as compatibility with existing ground receiving facilities to minimize costs.

The first design consists of a hardened hybrid package that is capable of providing sampled real-time data and high-resolution rate sensitive information in a nonreal-time mode. Design philosophy of this approach emphasizes telemetry performance margin and maximizes the probability of data retrieval regardless of the nature of the failure or resultant environment.

The alternate (unhardened) system provides real-time data and is lighter, smaller, and cheaper than the hardened system design. However, its diagnostic coverage is not comparable to that provided by the hardened system. Although the unit is somewhat limited by the frequency response and loss of signal in the event of a catastrophic failure, the resultant coverage is expected to suffice in the majority of cases.

Assuming the diagnostic coverage is deemed adequate, it is recommended that the real-time unhardened design be employed for those missions in which weight and cost considerations predominate. Conversely, for

mission applications in which weight and cost constraints do not preclude the realization of maximizing the probability of data return, the hardened hybrid system is recommended.

III. TECHNICAL APPROACH

The technical approach was first to review flight operations, systems, and user-related interface control techniques and to describe in general terms the characteristic needs, if any, for improved diagnostic instrumentation on future spacecraft during flight phases of solid propellant upper-stage and apogee motor burns. Additionally, the results and recommendations of prior failure review board reports were evaluated to determine critical parameters, resolution, frequency response, and accuracy requirements of diagnostic traces to be monitored during flight operations. Then the current work on solid motor instrumentation was surveyed through contacts with appropriate government agencies and private companies to augment the requirements evolving directly from this study.

Concurrently a technology review of existing instrumentation, data management systems, and surveillance and monitoring practices was conducted to serve as the basis of any future tradeoff studies. Target characteristics of advanced system designs were also established to form the basis of a meaningful comparison between competing systems. A failure modes and effects analysis was conducted to identify primary failure modes and discrete telemetry signals resulting from typical anomalies. Conceptual approaches to monitor and detect the occurrence of selective anomalies were formulated and evaluated with respect to technical feasibility and performance potential. Conceptual design analysis of the most promising approaches was conducted and the associated performance, cost, and unit characteristics determined.

To bound the problem, only the gross effects of typical spinning and nonspinning vehicles were considered; no attempt was made to rigorously treat the dynamics associated with spinning bodies nor the elastic coupling that exists between a spinning motor and despun payload or their effects upon selective telemetry signals. To facilitate this analysis and to arrive at a cost-effective configuration, design simplicity and the use of state-of-the-art technology were emphasized. The flight instrumentation module was

expressly designed to be self-contained and independent of the spacecraft, with the exception of initial turn-on signal. In one of the candidate designs, provisions were made to enhance the data link performance and probability of success of the SMDI package, even under the most severe dynamic spacecraft conditions and environment anticipated. The intent of this exercise was to evaluate the impact of these constraints upon overall performance, weight, and cost characteristics of the SMDI module.

The resulting designs were compared against competing approaches and their advantages and disadvantages determined. Based upon the foregoing analyses, the most promising systems were identified and recommendations made.

IV. TECHNOLOGY REVIEW

A. OVERVIEW OF TYPICAL FAILURES

Review board studies of typical solid motor failures were evaluated to determine probable causes of failure and to identify critical parameters and instrumentation requirements associated with diagnostic traces to be monitored during flight phases of solid motor burns. The findings of these investigations are summarized in Table 1 for representative apogee, upper stage, and retro solid motors selected as a basis of this study. As noted in the table, six specific motors were selected for the study to encompass the following spectrum of solid motor applications: (1) the SVM-1 was selected as being representative of the lower size limit of apogee motors, (2) the SVM-2 motor is middle sized and employs a composite motor case, (3) the TE-M-521 is representative of stretched spherical motors, (4) the TE-M-364-3 is typical of large spherical titanium-case motors, (5) the FW-4S is typical of the all-solid launch environment of the Scout and spin stabilization, and (6) the TE-364-1 is representative of three-axis stabilized retro motors employed earlier in JPL deep space missions.

Each of these motors was involved in an anomalous flight with varying degrees of flight instrumentation. In each case, other than the SVM-1 motor, failure "apparently" occurred over midway through the motor burn, near the interval of maximum acceleration. This suggests that acceleration-induced loads, coupled with other loads, might have played a role in precipitating the ultimate failure. Additionally, qualification test procedures did not include

the requirement for the application of static acceleration in combination with other launch phase loads or the application of static acceleration during burn. Thus, some questions remain as to the margin of safety provided to the motor designs under combined service loads.

Note also that the failure associated with the SVM-1 motor (Intelsat II spacecraft) appears to be the only one whose probable cause (low temperature excursion) was explained beyond reasonable doubt. In each of the other incidents, the probable causes of failure postulated are highly speculative in that the extent of telemetry data available to support these hypotheses are generally recognized as being far from adequate. The Surveyor IV flight is a departure from this norm as it represents the most highly instrumented failure documented to date. However, the findings of the failure review board were also inconclusive as to probable cause of failure owing to the nature of and abrupt loss in telemetry signals.

In order to test the correlation and/or influence that prelaunch operations may have contributed to the failure of these motors, the requirements and irregularities observed during the lifetimes of these devices were examined. Pertinent data delineating the requirements, rejection criteria, and anomalies reported for each of these motors are summarized in Table 2. (A further delineation of specification requirements is presented in the Appendix.)

Of significance from Table 2 is the evident lack of requirements for the control and verification of storage and transportation environments that is prevalent among these solid motors (the SVM-1 motor is the only departure from this trend). For example, the SVM-2 motor was stored at three different locations; one of them being at San Juan Capistrano, California, where it was stored for a period of one year without environmental control or monitoring. Note also that the total time interval between manufacture and service use was relatively long and exceeded specified requirements in two cases. The significance of this anomaly is further amplified in light of the findings of the parallel study (Ref. 19) that related direct correlation of failure rate to solid motor lifetime.

B. EXISTING MONITORING AND SURVEILLANCE PRACTICES

1. Ground Handling

Monitoring and surveillance practices presently observed during ground handling have matured significantly in recent years. Where the employment of recording instruments to monitor temperature, humidity, vibration, and shock was an exception rather than the rule, their current use is a matter of increasing routine. Utilization of temperature and humidity controlled air-ride vans to transport the solid motors from manufacturer to launch site is also becoming common practice. Storage provisions at the launch site offer adequate thermal- and humidity-controlled environments. The inadequacies, if any, that exist during ground handling, transportation, and storage lie in implementing adequate control and monitoring practices; not in the absence of any suitable instrumentation or recording devices.

2. Flight Operations

In contrast to ground handling, the primary flight instrumentation problem stems from the inadequacies or lack of adequate instrumentation coverage that is or can be dedicated to propulsion system diagnostics. Accordingly, the main thrust of this study focused upon the definition and design analysis of flight instrumentation packages capable of providing suitable diagnostic information with minimal penalty to the parent spacecraft.

To this end a review of monitoring and surveillance practices employed in typical spaceflights to date was conducted. The results of this investigation revealed that the extent of flight instrumentation devoted to monitoring solid motor diagnostic information has varied significantly (0 to 5 channels of on-board instrumentation) depending upon the ultimate user. Although the desirability or recognition of need for additional diagnostics is prevalent among propulsion system designers, an inadequacy arises in most flights as a result of the hierarchy assigned to the total spacecraft data management system. For those flights in which solid motor measurements were retained, the coverage was still considered inadequate due to the commutated nature of the signal, sampling rate, or rapidity of failure mode.

NASA has historically adopted a more conservative view and the extent of on-board instrumentation that has flown on typical missions (although somewhat limited) is a reflection of this posture. The IMP H, Surveyor, and Pioneer missions are representative examples of the attention focused

upon upper stage solid motors. In contrast, recent missions flown by the military and commercial organizations have indicated a tendency to de-emphasize the need for propulsion system diagnostics.

A survey of current users has uncovered an emerging recognition for the need to improve flight diagnostic instrumentation. The NATO-III satellite is a typical example of this evolving philosophy. But here, again, the extent of on-board diagnostics is expected to be limited to a chamber pressure (P_c) gauge (Standard Controls 213-35-280-02 pressure transducer) supplying low rate commutated data (2 samples/s) during the actual burn and thermocouples to substantiate prefire thermal conditions about positions of significant mass. Although the need for continuous real-time data was recognized, the ultimate sampling rate was selected on the basis of overall spacecraft considerations.

The findings of failure review boards have clearly indicated that the extent of transmitted data is far from adequate for identification of possible failure modes. In addition, there are no missions within the immediate planning horizon in which any significant relief from this predicament can be anticipated.

3. Typical Flight Operations Case Histories

Additional expository remarks on two typical missions will be presented to further amplify upon existing flight surveillance practices. The first example is the retromotor used on the Surveyor spacecraft in which the Hughes Aircraft Company was the prime contractor. The burning of the Surveyor retromotor, an event which took place some 97 km above the surface of the Moon, was monitored by an accelerometer, a pressure sensor, and three temperature sensors. Engineering and science telemetry shared a common S-band telecommunications link. Although there were multiple transmitters and multiple antennas, only one spacecraft-to-ground communications channel could be active at any one time. Continuous data on some devices were available; however, this capability was not employed on the retromotor, as all retro data were commutated (Ref. 20).

The Surveyor vehicle contained seven strain gauge force sensors, one of which was attached to the outer metallic surface of the spherical motor, to measure chamber pressure of the retromotor. The output of the strain gauge was conditioned by the strain gauge amplifier assembly to a standard

level of 0-5 V and the scale factor was $1040 \text{ N m}^{-2} \text{ V}^{-1}$. In the signal processor, the retro-pressure signal was commutated, digitized, and incorporated into the time-division multiplexed data stream for transmission to ground.

Acceleration along the roll (thrust) axis was sensed by the retroaccelerometer of the spacecraft during the firing of the retromotor. The sensor was of the potentiometric type, where a seismic mass is linked to the wiper of a potentiometer having an output signal proportional to the force acting upon the mass. This type of sensor has a slow response (e. g. , 10 to 20 Hz) which limits the diagnostic information that can be obtained. The accelerometer output signal (0 to 5 V, scale factor = 0.333 V/g) was commutated and digitized by the signal processor and incorporated into the time-division multiplexed data stream. The retroacceleration signal was supercommutated (four words per frame) to increase the number of samples obtained during the motor burn of approximately 47 s.

The Surveyor vehicle had a total of 74 resistance-type temperature sensors. Three of these were on the retromotor: upper retro case, lower retro case, and retro nozzle. These sensors were of the type in which a constant current (2.5 or 5.0 mA) is passed through a known resistance producing a voltage signal proportional to its temperature. The output signal (0 to 5 V) was routed to the signal processor where it was commutated, digitized, and incorporated into the time-division multiplexed data stream.

Burner II by the Boeing Company is the second example in which the stage is equipped with a telemetry system designed to isolate the source of malfunctions in the major subsystems (Ref. 21). The telemetry subsystem is of the FM/FM type, operating in the VHF band. Sensors which could be used to assess rocket motor performance include an accelerometer and pressure transducer. The output of the accelerometer was conditioned to a level of 0 to 5 V and fed to a subcarrier oscillator operating on IRIG Channel C which has a center-frequency of 40 kHz, a maximum frequency response of 6.0 kHz and a maximum risetime of 58 μs . The system can indicate accelerations somewhat above this rate, but the response of the sensor to low-frequency accelerations is not known.

Correspondingly the output of the Burner II pressure sensor is conditioned to the 0 to 5 V level, sampled by a 30-segment 10-samples/s-commutator and fed to a channel A (22 kHz) subcarrier oscillator.

Rocket motor monitoring provisions for the Surveyor spacecraft and Burner II stage are tabulated in Table 3. In addition to the differences which have been noted in the two spacecraft telemetry designs, Surveyor and Burner II used different types of radio facilities at the receiving end. Being an integrated system (science and engineering), Surveyor telemetry was received at the specialized NASA deep space receiving stations. Burner II, being an independent general-purpose vehicle, directed its telemetry to the standardized IRIG test range instrumentation net.

C. AVAILABLE INSTRUMENTS

Flight diagnostic instrumentation packages generally employ three types of transducers in order to measure pressure, acceleration, and temperature. In many instances the same instruments can be used for both flight and ground test applications. All require amplifiers to boost their outputs to prescribed "standard" levels for application to telemetry systems. In addition, most of them require a biasing current or voltage to produce an output.

Pressure sensors and accelerometers can be of similar design because they both measure force. Those that need to follow high-frequency inputs are of two general types, i. e., piezoelectric crystal and strain gauge. The crystal type needs no bias (depending upon the piezoelectric effect) as a proportional voltage is generated across the crystal in response to applied pressure. Additionally, crystal sensors exhibit excellent frequency response, but they have a high source impedance which complicates their integration into a spacecraft system. The amplifier and the cable connecting the amplifier to the sensor must maintain input impedances of $10^{13} \Omega$ and, in some cases, the capacitance of the connecting cables must be extremely stable (Ref. 22).

The other type of high-frequency force sensor, the strain gauge, is more amenable to flight use because it has a low source impedance. Strain gauges are used as one or more resistance elements in a resistance bridge. Temperature compensation capability is built into the bridge configuration design. The bridge is biased with a constant current or constant voltage and

produces an output current or voltage which is proportional to applied force. Strain gauges can be of several types, the latest using thin-film semiconductor technology. These are formed by vacuum deposition on the force-sensing element of the transducer. This represents a pressure diaphragm in the case of a pressure sensor and a grid and seismic mass in the case of an accelerometer. Due to the low source impedance of a strain gauge bridge, a simple amplifier with conventional wiring can be used to couple the output signal to the telemetry system. The strain gauges are very small, are produced by microcircuit techniques, and result in sensors of very high natural frequencies (Ref. 23). The design characteristics of typical sensors used to monitor motor performance are given in Table 4. Many of these devices are miniaturized with little or no apparent loss in performance characteristics. For example, the pressure transducer P14E¹ listed in Table 4 has a 0.25-cm-diam diaphragm, a natural frequency of 175 kHz, and maintains its rated accuracy up to 35 kHz (Ref. 24).

Remote temperature sensing can be done with thermistors, thermocouples or linear resistance elements. The latter is used at JPL extensively because of the accuracy which can be obtained with a linear element and the overall simplicity of the circuit. The sensing element is a thin platinum wire through which a small, constant current is passed. Resistance of the platinum wire, and hence the voltage developed across it, is a function of the temperature of the wire. Output voltage is boosted to the standard telemetry level by simple amplification. Typical physical dimensions for a resistive temperature sensor are $0.5 \times 0.38 \times 0.15$ cm for a unit to be attached by bonding and $2.5 \times 2.5 \times 0.25$ cm for a bolted unit (Ref. 25). Choice of mounting method is dependent upon the expected temperature range.

V. SMDI REQUIREMENTS

A. SYSTEM REQUIREMENTS AND OBJECTIVES

As previously noted the primary objective of the SMDI system is to provide capabilities to: (1) detect whether or not the solid motor was the

¹The Air Force Rocket Propulsion Laboratory is investigating pressure sensors of this type to be implanted within the vessel being instrumented (e.g., under the insulation of a rocket motor).

cause of failure, and (2) identify probable primary failure mode(s). To meet these objectives a requirements and failure modes and effects analysis was conducted to identify functional and desirable unit characteristics, candidate conceptual approaches, and diagnostic performance potential.

A survey of potential users and the conducting of a requirements analysis resulted in the formulation of the following functional requirements.

- (1) Detection of an event or anomaly within 16 μ s.
- (2) Near-Earth operation (\leq synchronous orbit).
- (3) Operational cycle \cong 120 to 180 s real-time.
- (4) Transmission on standard Inter-range Instrumentation Group (IRIG) frequencies.
- (5) Continuous data transmission without attitude constraints.
- (6) Maximum g loading \leq 30 g (unhardened system)
 \leq 10,000 g (hardened system)
- (7) Rate sensitive acceleration and chamber pressure measurements are acceptable where analog traces are not practical.
- (8) Real-time mensuration characteristics of the required instruments as given in Table 5.
- (9) Thresholded data system requirements as summarized in Table 6.

Many of the requirements presented in Tables 5 and 6 are given by worst-case conditions or sensitivities necessitated for the detection of high frequency or short duration events. For example, the frequency response designated for the P_c trace (\geq 5 kHz) is a minimum sensitivity necessary to detect the occurrence of combustion instability. Similarly, frequency response of the orthogonal accelerometers is selected to detect "chuffing" in the event of case burnthrough. The consensus of opinion encountered for accuracy and resolution requirements of these devices ranged from $\leq \pm 1\%$ end-to-end to any reasonable value, provided the frequency response was adequate to detect the required rate sensitive anomalies. The characteristics of the temperature probes are least demanding because of the slow response of thermal delta functions. Thus, the primary function of these devices reduces to the verification of acceptable prefire thermal soak conditions. Although additional data are possible from this instrument during an

actual motor burn, to ensure a high probability of achieving additional diagnostic coverage would entail the integration of an excessive amount of temperature pickups.

To provide a meaningful basis of comparison between competing systems, the following additional set of ground rules and constraints were established:

- (1) Self-contained SMDI package
- (2) System weight ≤ 5.4 kg (12 lbm) [2.3 to 4.5 kg (5 to 10 lbm) target]
- (3) Volume ≤ 0.014 m³ (0.5 ft³)
- (4) Recurring cost \leq \$50K (~\$20K target)
- (5) Both hardened (low data rate) and unhardened system configurations are acceptable

The selection of these added constraints was based upon the following rationale. To minimize the impact of integrating the SMDI package, the module was required to be self-contained, with the exception of turn-on and motor ignition signals from the parent spacecraft. This feature further removes the probability of a loss in telemetry signal in the event of a failure in the spacecraft telemetry or power subsystem. Target values for system weight and costs were established, based upon estimates of what typical missions could bear. The volume requirement is not expected to be a primary parameter, unless mission-peculiar constraints dictate otherwise. To evaluate the penalties of enhancing the probability of acquiring diagnostic data in the event of a catastrophic failure (i. e., blow of motor), both hardened and unhardened configurations of the SMDI package were considered.

Candidate conceptual approaches were accordingly reduced to an unhardened high data rate continuous real-time system and a hardened thresholded hybrid system. The latter combines the characteristics of a thresholded and commutated real-time system. The relative merits of such a system includes the benefits of acquiring extremely accurate rate-sensitive data as well as a cursory indication of the general waveform prior to, during, and following the occurrence of an anomaly.

Physically, the spacecraft-mounted solid motor diagnostic instrumentation system is divided into two major elements. These are: (1) the

external sensors located at various locations in the vicinity of the motor to enhance intensity and detection of discrete signals, and (2) the critical data recorder (CDR) package that is remotely situated at a position favorable for transmission. The external sensors consist of accelerometers, pressure transducer, and temperature sensors which provide analog signals to the CDR for processing and storage. Further exposition of the competing systems is presented in Section VI.

B. FAILURE MODES AND EFFECTS

A failure modes and effects analysis was conducted to examine the degree of detection and discrimination potential that each of the candidate approaches offered. A compilation of primary failure modes, potential causes of failure, effects, and resultant telemetry signals for an unhardened continuous real-time system is presented in Table 7.

As noted in the table, the study evaluated five primary failure modes: blow of the motor, nozzle failure, case burnthrough, failure or interruption of ignition, and combustion instability. Included in the table is a summary of statistical trends established for each of these failure modes in previous malfunction system studies (Refs. 26, 27). It is significant to note that aside from ignition malfunctions, all other types of failure could occur at any time during the motor burn. Additionally only a small fraction of motor failures occurred with no prior indication of malfunction. Provided the sensitivities and data rates are of sufficient magnitude, no major deficiencies in diagnostic capabilities are anticipated for the continuous real-time system.

A possible exception could result from the incidence of a catastrophic failure with no prior warning. However, by selectively deploying the probes and assessing the order or sequence of signal loss, a great deal of intelligence regarding the probable primary failure modes can be gleaned. For example, by judiciously shielding and displacing the accelerometers away from the motor, the sequence of signal loss can be ordered between the chamber pressure and accelerometer traces. The loss of the temperature traces should be random, depending upon the proximity of transducers and lead wires to the position of case rupture. Notwithstanding, the use of doppler data, in conjunction with high sensitivity accelerometer information, should provide an adequate basis for substantiating the possibility of a blow to the motor.

A similar compilation for a thresholded system was prepared and is presented in Table 8. Of significance is the discrete character of each of the typical diagnostic traces that facilitates failure mode differentiation. From the acquisition of commutated real-time, timed, and untimed data, the general waveform (including initial rise time) of each of the traces can be determined. In addition, any anomalous rate-sensitive exceedance data can be determined accurately (within 16 μ s) by actuation of multiple threshold indicators (i. e., timed events). Durations for premature combustion termination and prolonged burns can also be determined to equivalent precision by the actuation of low-level trips. Finally, the added capability to precisely detect and measure the effects of oscillatory combustion in both the chamber pressure and transverse accelerometer pickups provides an added dimension in diagnostic monitoring and surveillance capabilities.

Combustion instability has received intensive interest in recent years as a result of persistent developmental problems experienced in rocket engines. The criticality of oscillatory combustion in solid-propellant rocket motors is particularly intense and continuing research is being devoted to the understanding of underlying basic physical principles associated with this phenomenon. Of interest to this study is the detection of high-frequency instabilities that could conceivably lead to increase in burn rate (resulting in case burnthrough), grain breakup, and rough ride.

The other oscillatory combustion phenomenon of interest is "chuffing." Its occurrence may stem from case burnthrough or other events that significantly reduce chamber pressure. Chuffing is a low-frequency oscillation that can give rise to incomplete combustion, premature extinguishment, and deterioration of propulsive performance. The detection of these oscillatory combustion phenomena should materially assist in providing added insight into the probable cause of failure and in identifying areas for future technology development.

In summary, for both of the candidate approaches, the use of information gathered from the SMDI module, in conjunction with those data obtained from standard spacecraft/ground telemetry systems, should provide an adequate basis to postulate motor failure and probable failure modes.

VI. CONCEPTUAL DESIGN

A. HARDENED CDR DESIGN

1. Design Criteria

The following design criteria were established to form the basis for the hardened design of the CDR:

- (1) The CDR must be cost effective. Therefore, the design must emphasize simplicity and minimize required development. Accordingly current state-of-the-art techniques and hardware will be employed throughout.
- (2) The CDR will be electrically independent of the spacecraft with the exception of initial turn-on and motor-ignition signals. It will therefore have its own fully self-sufficient telemetry system and power source.
- (3) The CDR package will be capable of surviving shocks of up to 10,000 g for a duration of 30 μ s. This will protect the CDR against typical impulsive loads resulting from a motor explosion.
- (4) The total weight of the CDR package exclusive of external sensors and wiring shall be less than 5.45 kg (12 lbm).
- (5) The telecommunications system of the CDR will be designed for maximum data link performance to increase the probability of CDR success under abnormal spacecraft conditions and/or environment.
- (6) The CDR will have no uplink capability.
- (7) The CDR will be turned on by a spacecraft-generated signal just prior to motor ignition. Following turn-on, the CDR will cycle itself, independent of the spacecraft, through all of its required modes of operation.
- (8) During the acquisition of diagnostic data, the CDR will be capable of transmitting sampled real-time sensor measurements to provide supplementary information describing preignition status and overall waveform characteristics of signals monitored.

- (9) Following the accumulation of diagnostic data, the CDR will sequentially transmit a minimum of two complete data frames over each of several antennas, assuming that only one will have an acceptable pattern with respect to Earth.
- (10) Real-time demodulation of the data following RF detection on the ground will not be required.

2. Design Description

The hardened CDR is capable of downlink transmission in two operational modes: nonreal-time data and sampled real-time data modes.

a. Non-Real Time Data Mode. The CDR is a specialized telemetry system which uses a high degree of data compression to efficiently monitor the flight performance of solid rocket motors. After being initiated, it is entirely independent of all other subsystems, including power and radio, so that anomalies in propulsion can readily be distinguished from anomalies in other areas. The CDR concept provides for recording motor data at a high rate during the motor burn and transmitting it to Earth at a low rate after the burn to maximize the communications link performance. The system is designed to withstand catastrophic disintegration of the spacecraft and faithfully transmit all data received during its programmed recording period — 512 s from initial turn-on (T_0).

The CDR accomplishes data compression by recognizing and recording the passing of predetermined thresholds, called "events." There are two classes of events, "timed events" and "untimed events." Timed events are identified and time-tagged relative to time T_0 with a resolution of 16 μ s. If multiple timed events occur within the minimum resolution of 16 μ s their order of occurrences is preserved. Table 9 lists the 29 timed events provided for the model system. Its instruments consist of a triaxial accelerometer, a pressure sensor, and two temperature sensors. The events defined yield information associated with the rise time, excursions, oscillatory event frequency and amplitude, overall duration of acceleration, and temperature and pressure profiles. Untimed events are identified and labeled as to occurrence or nonoccurrence. Table 10 lists the 51 untimed events provided for the model system. The portion of the CDR which accomplishes the above data recognition, timing, and storage is called the data encoder.

Figure 1 is a block diagram of the complete CDR. The blocks form a self-sufficient system, requiring only the input of analog signals from the SMDI sensors, and a start command from the spacecraft programmer. The solid motor ignition command is a convenient start command. Conditions being sensed at that instant, and subsequently will be recorded.

The key operations which are performed by the data encoder section are: timing and control, event detection, and memory. The timing and control section within the data encoder provides a fundamental clock frequency from which all other timing and synchronization signals are derived by dividing down. Control circuits utilize the timing signals to transfer data to and from the memory and to perform mode changes.

Event detection is performed by comparing the analog outputs of the various sensors with preset reference voltages. When a timed-event threshold is sensed, the threshold's identification (Table 9) and the time of its occurrence are read into the memory. When an untimed-event threshold is sensed, the fact of its occurrence is read into the memory.

The CDR incorporates a 1536-bit semiconductor memory, of which 1305 bits are available for storage of data for the SMDI sensors. Each of the 29 timed events comprises a 30-bit memory word, 5 bits for identification and 25 bits for time-tag (Fig. 2). Each of the untimed events is represented by a single bit. The data frame (contents of the memory) is read out twelve times at the conclusion of the recording period to assure reception by the ground station.

Typical electronic circuitry to detect oscillatory event occurrence, frequency, and amplitude is described in Fig. 3. The mechanization of this diagnostic capability is effected as follows. The sensor output signal is compared with a reference voltage about which the oscillations will occur. This reference voltage is achieved by simply passing the sensor output through a low-pass filter or integrator. This voltage is then applied to the analog-to-digital converter (ADC) where it is converted to a 7-bit word providing 0.8% resolution. The multiplexed sensor line would be temporarily inhibited with the occurrence of an oscillatory event pulse and the ADC used to digitize the amplitude of the oscillatory signal. The resultant 7-bit data word could also be identified and inserted into the real-time data stream if

desired. This would provide information in real-time that oscillations in that particular sensor are occurring and to what amplitude.

Radio transmission from the CDR is by frequency shift keying/phase modulation (FSK/PM) in the S-band (2200 to 2300 MHz). The choice of transmission was based on performance efficiency and compatibility with existing ground receiver sites. FSK/PM is amenable to both coherent and noncoherent reception, permitting the ground station to use coherent real-time detection and predetection recording simultaneously for redundancy. A data transmission rate of 4 bits/s and a transmitter output power level of 200 mW has been selected to minimize the SMDI power requirements.

The transmitter consists of the necessary elements to accomplish the generation and modulation of the RF carrier signal. A crystal-controlled solid-state oscillator is used to generate the fundamental frequency from which the final output frequency is derived through frequency multiplication. Two types of frequency multipliers are employed to condition the initial and resulting intermediate frequencies: (1) lumped-constant, varactor frequency multipliers and (2) stripline, varactor frequency multipliers. Three solid-state power amplifiers are also included in the proposed transmitter design. Their purpose is to provide sufficient interelement gain, isolation, and harmonic rejection so that the required transmitter output level and quality can be achieved.

The modulation function is accomplished through the use of a Varicap phase modulator. At an intermediate carrier frequency of 63.6 MHz, a time-variant voltage level is translated into the required phase deviation. The time-variant voltage, received from the data encoder subsystem voltage-controlled oscillator (VCO), coupled with the modulator sensitivity will determine the degree of carrier suppression and sideband frequencies. The transmitter output element consists of a stripline ferromagnetic isolator that was expressly selected to provide minimal insertion loss to the incident output signal and a very high isolation from undesired reflected output signals.

The antenna system consists of six impact-resistant integrally mounted antennas, each facing in a different direction. To permit the use of a small low-powered transmitter, the transmitter is connected to one antenna at a time by means of an antenna selector switch. The radiation pattern from each antenna is right-hand circularly polarized. During the data transmission

period, control circuits in the data encoder select each antenna in turn and cause the contents of the memory to be transmitted twice over each of the six antennas. This process, which takes approximately 1 hr, assures reception of the data by the ground station without regard for the orientation of the spacecraft and/or CDR during this time interval.

Electrical power for all functions of the SMDI is supplied by two silver oxide-zinc primary batteries. A 28-V battery supplies power for the transmitter and data encoder modulator, while a 10-V battery supplies power for the logic and control functions. Voltage regulation is necessary in only one area, the reference voltages.

The operation of the SMDI can best be understood by following the sequence of events from turn-on (T_0) to turn-off. Turn-on is initiated by a signal from the spacecraft sequencer. All subsequent events are referenced timewise to the instant of turn-on. Power is applied to all circuits which are utilized in the data acquisition mode. Counting is initiated by the timing generator. All threshold detectors are set to their lowest levels. When any timed-event thresholds are sensed, the events are identified, time-tagged, and stored in memory; those threshold detectors are then cycled to their next higher levels. Later, the negative-slope threshold detectors are triggered and the associated data stored. At the same time the untimed-event detectors are filling an untimed-event register as their thresholds are exceeded. When the timing generator senses that 512 s have elapsed, the data acquisition period ends. The contents of the untimed-events register are transferred to memory.

Coincident with the cessation of data acquisition, power is applied to the radio and the transmission mode begins. The contents of the memory are transmitted twice over the first-selected antenna at the rate of 4 bits/s. The control section then selects the next antenna and the contents of the memory are again transmitted twice. As each new antenna is selected, sufficient time (88 s) is allowed for the ground receiver to establish "lock" on the signal before continuing data transmission. When all of the data has been transmitted twice over each of the six antennas, SMDI power is turned off to avoid possible interference with the spacecraft system.

b. Real-Time Data Mode. The resultant reduction in quantity of data and data rate arising from the nonreal-time system (in comparison with

a conventional real-time system) provides a significant improvement in communications link performance capability and, thereby maximizes the probability of an acceptable data return. However, the minimization of data through selectivity of critical event data only, by necessity, excludes some information that could be useful. To alleviate this problem area, additional real-time information describing preignition status and overall data waveform characteristics are transmitted to supplement the selected critical event data. Such fill-in data does not have to be returned at a high bit rate, but could be provided by real-time transmission of the sampled sensor outputs at the nominal bit rate selected for nonreal-time transmission. Such real-time transmission would begin just prior to motor ignition and continue through the 512-s nonreal-time event data acquisition period.

The mechanization of real-time data transmission is readily accomplished since the data encoder, VCO, and transmitter are available during this period, and the only addition to the existing electronics involves the real-time data processing circuitry. As noted in Fig. 4, the required data processing consists of one analog multiplexer for time-multiplexing the six sensor outputs and one ADC to accomplish the required analog-to-digital conversion prior to FSK modulation of the VCO subcarrier.

No antenna switching is assumed for the real-time data mode. During installation, one of the six antennas would be selected for real-time transmission. This would normally be the antenna pointing in the same direction as the spacecraft-mounted antenna. Assuming nominal spacecraft performance, this should provide the most favorable communications path. The antenna switch corresponding to the selected antenna is activated with power turn-on and, therefore, controls the transmission path for the first two frames of nonreal-time data. The sequencing through the remaining antennas is employed for the nonreal-time data mode only to compensate for losses due to possible changes in spacecraft orientation resulting from the motor burn.

Assuming a nominal 4 bits/s data rate for the real-time mode and 7-bit (0.8%) resolution, each of the accelerometers and the pressure transducer

are sampled every 7 s during the 512-s real-time transmission period, while the slowly varying temperature measurements are sampled every 70 s.²

3. Performance Analysis

A performance analysis has been conducted to demonstrate that a positive margin exists in the CDR-to-Earth communications link. Radio transmission parameters, radio reception parameters, and telemetry parameters used in the analysis are listed in Tables 11, 12, and 13, respectively. The CDR telecommunications link design analysis is summarized in Table 14.

For clarification purposes, the following definitions are applicable to the interpretation of Table 14.

- (1) Performance Margin: the ratio of the nominal received signal level (carrier or modulation) to the nominal threshold signal level expressed in decibels. It is considered acceptable when the margin is positive and equal to or greater than the magnitude of the linear sum of the adverse system tolerances.
- (2) Nominal Received Signal Level: the received signal level as calculated from the nominal system parameters (gains, losses, and power levels). The calculation excludes (for all practical purposes) arbitrary margins, pads, or unknown factors.
- (3) Nominal Threshold Signal Level: the received signal level required to achieve a threshold signal-to-noise ratio in the effective noise bandwidth of a detector or demodulator given the system noise spectral density.
- (4) Threshold Signal-to-Noise Ratio: the signal-to-noise ratio required at the detector that will result in the minimum acceptable system performance.

The assumed parameters (data rate, transmitter power, etc.) defined in Tables 11, 12, and 13 yield an acceptable subcarrier performance margin of 26.3 dB.

²It should be noted that the ultimate performance margin computed (26.3 dB at 4 bits/s) allows significantly higher sampling rates to be employed if required.

4. Design Characteristics

The mechanical design of the CDR, is shown in Fig. 5. It consists of a rigid sectional metal structure housing four major modules. These comprise: (1) the data encoder, (2) the batteries and transmitter, (3) an upper antenna assembly, and (4) a lower antenna assembly. The upper antenna module contains five integral foam-filled printed-circuit antennas located 90 deg apart. The lower antenna module contains a single additional antenna.

To protect against impulsive loads the metal structure will be covered with a layer of balsa wood and then a layer of fiberglass. Thermal control will be provided by an RF-transparent Mylar blanket. The total weight and volume of the CDR assembly, including impact limiter and thermal control, are 4.67 kg (10.3 lbm) and 0.0097 m³ (592 in.³), respectively (Table 15).

Power consumption during the CDR mission is shown Figs. 6, 7, and 8 for the nonreal-time and real-time and real-time data modes, respectively. Total consumption from the 28-V battery is 4.33 W-h, and from the 10-V battery is 0.43 W-h. The nominal energy ratings of the 28-V and 10-V batteries are 6.7 W-h and 2.4 W-h, respectively.

5. Design Option

The previously described hardened design for the CDR assumes sequential transmission of a minimum of two complete data frames over each of six antennas following the acquisition and storage of critical data during the motor burn period. This is based upon the possible occurrence of an unpredictable change in the spacecraft orientation where only one antenna may have an acceptable pattern with respect to Earth. Simultaneous transmission from all antennas was not included in the initial hardened design due to the attendant losses involved. Power division between six antennas would introduce an 8-dB loss alone, while radiation pattern nulls resulting from destructive interference between antennas could introduce losses up to 15 dB in certain directions. Although the latter effect could possibly be compensated for by diversity reception techniques at the IRIG receiving stations, it does pose an added complication.

The highly efficient sequenced mode should suffice for 90% of the solid motor firings; however, it does not guarantee a continuous coverage pattern from any one antenna under all conditions associated with a catastrophic failure wherein the spacecraft and/or CDR are placed in a tumbling mode.

Because multiple frames are transmitted from each antenna and a nonreal-time noncoherent detection process is available, most of the data would probably be retrieved. The success of this approach, however, would be contingent upon putting together pieces of received information to form the whole on a best endeavor basis.

Since the telecommunications performance margin of Table 14 reflects a +26.3-dB margin, the simultaneous mode of radiation appears attractive as a follow-up to the sequenced mode to protect against potentially intermittent antenna coverage conditions associated with a tumbling mode. In this operational approach the data encoder would switch the CDR to the simultaneous radiation mode following sequential transmission of two frames of data through each of the CDR antennas. With the existing performance margin, the losses and nulls should be tolerable so that information would be continuously received. Again, even though nulls might cause a loss of lock, the previously described process for predetection recording of the signal would allow the critical data to be noncoherently extracted from the tape by computer spectral techniques.

The power limitations associated with this option are contingent upon the design capability of the battery which provides the 28-V power to the transmitter. The predicted 1.9 W-h margin will more than accommodate the expected power consumption of the simultaneous antenna radiation mode. The power required during this mode will be essentially the same as for the sequenced mode, i. e., 4.23 W. Assuming a drain of 4.23 W following the sequential mode, an additional 0.45 h (27 min) of radiation can be achieved before the battery rating is exceeded. Based upon the data requirements projected in Fig. 2 for a typical CDR data frame, several complete frames of data could be transmitted in the simultaneous radiation mode with the present design.

6. Costs

The CDR design approach defined herein was based upon the use of proven techniques and already developed hardware to minimize development costs. For example, the proposed 10,000 g high-impact transmitter design has already been successfully developed and tested by JPL under NASA advanced development sponsorship (Ref. 28). Similarly, the foam-filled integral cavity-backed printed circuit spiral antenna design has been

developed and successfully tested by JPL at 5,000, 8,000, and 10,000 g (Ref. 29). The data encoder design, although unique to this application, employs conservative and straightforward design techniques based upon the use of presently available production line components which only require the application of suitable packaging techniques to meet the specified CDR environmental requirements. Furthermore, the CDR power requirements have been minimized so that the battery can be implemented using conventional and presently available cell designs.

A breakdown of estimated costs associated with the development and production of flight units is presented in Table 16. It is anticipated that the \$240K CDR development effort could be implemented within ~8 months. It should be noted that the typical cost for a flight quality unit (estimated at \$45K) is based upon production quantities of 50 to 100 units. This is intended to capitalize upon the economy of lot size.

It should be further noted that the foremost cost-pacing item associated with both the CDR development and production is the transmitter. The capability to survive 10,000 g dictates a level of precision, quality assurance, and testing which directly controls the cost. Relaxation of performance and environmental survival requirements could affect the transmitter production costs by as much as 50%.

In addition, the overall CDR design described in this report possibly reflects an overly conservative design which could be significantly simplified and still achieve the basic mission requirements with an acceptable probability of success. For instance, the large telecommunications link performance margin might allow the number of antennas to be reduced from 6 to as few as 2 or 3. Furthermore, if simultaneous radiation from all antennas is considered acceptable from a link performance standpoint, the antenna switches and associated switching circuitry could possibly be eliminated. Such simplifications, although resulting in a degraded performance margin and higher risk, could reduce the CDR production costs by as much as 20%.

B. UNHARDENED CDR DESIGN

1. Design Criteria

The following design criteria established the basis for the unhardened CDR design:

- (1) The CDR will be targeted for a production cost equal to or less than one-half that defined previously for the hardened design.
- (2) The CDR will be electrically independent of the spacecraft with the exception of the initial turn-on signal. It will therefore have its own self-sufficient telemetry system and power source.
- (3) The CDR package design will not be hardened to survive and/or perform during catastrophic failure modes when high-g shocks or spacecraft tumbling are expected to occur.
- (4) The total weight of the CDR package, exclusive of external sensors and wiring, shall be less than 2.27 kg (5 lbm).
- (5) The telecommunications system of the CDR will be designed for maximum data link performance to increase the probability of CDR success under abnormal spacecraft conditions and/or environment.
- (6) The CDR will have no uplink capability.
- (7) The CDR will be turned on by a spacecraft-generated signal just prior to motor ignition.
- (8) Following turn-on, the CDR will sample each of the data sources at the highest practical rate and transmit the information back to Earth in real-time throughout the period of motor burn. Pressure transducer data will require a 5-kHz frequency response and 5% accuracy, while accelerometer data will require a 2-kHz frequency response and 5% accuracy.
- (9) The CDR telecommunications systems will be fully compatible with existing IRIG station equipment and capability.

2. Design Description

The proposed CDR structural design is shown in Fig. 9. It consists of a rigid sectional metal body housing two modules. These contain: (1) the

data encoder, radio, and power supply; and (2) the antenna. In this design, the antenna assembly consists of a single antenna. To provide thermal control, the CDR is insulated with an RF-transparent Mylar blanket.

The data encoder section of the CDR consists of three subsections: (1) timing and control, (2) analog multiplexer, and (3) the modulator. All CDR timing functions are derived from a central oscillator and divide-down chain in the timing and control subsection. An analog multiplexer sequentially selects the outputs of the external sensors in accordance with a predetermined format. This format provides for sampling the pressure sensor at the rate of 10,000 samples per second (sps), each of three accelerometers at the rate of 4000 sps, and each of two temperature sensors at 1000 sps. The modulator is a voltage-controlled oscillator operating at a center frequency of 165 kHz. The output of the multiplexer (which is the combined data stream from all the sensors) frequency-modulates the VCO. The VCO then phase-modulates the CDR transmitter.

The radio subsystem is a solid-state 10-W telemetry transmitter operating in the S-band (2200 to 2300 MHz).

The antenna subsystem is a single-integral cavity-backed, printed-circuit antenna with an associated cable. Its radiation pattern is right-hand circularly polarized.

All power required by the CDR is provided by the power subsystem. A 28-V primary silver oxide-zinc battery with a 10-V tap comprises the power source. The transmitter and VCO require 28 V, and 10 V is required by the logic circuits. Total energy requirement is approximately 10 W-h.

The sequence of events for the CDR commences with its being turned on by an external command, such as a signal which coincides with the ignition signal to the solid motor. Outputs of the sensors are sampled at the preset rates previously noted and transmitted to Earth in real-time. At the end of 512 s the CDR is turned off to avoid interference with other systems on the spacecraft.

3. Performance Analysis

The values of the principal parameters which were assumed in order to establish the overall CDR telecommunications link performance are defined in terms of the signal-to-noise ratio in Tables 17, 18, and 19. The

CDR telecommunications design control table for the spacecraft-to-Earth link is presented in Table 20. Performance analysis was based on a maximum communications distance of 40,200 km (25,000 miles). Definitions of the terms: performance margin, nominal received signal level, nominal threshold signal level, and threshold signal-to-noise ratio are identical to those cited previously in Section VI-A.

The parameters defined in Tables 17, 18, and 19 yield an acceptable subcarrier performance margin of 5.8 dB.

4. Design Characteristics

The unhardened CDR design consists of a mechanically integrated arrangement of two modules connected together with eight titanium bolts. A modular breakdown of the CDR mechanical structure is illustrated in Fig. 10. It should be noted that the data encoder, radio, and power subsystems are contained within one subassembly module.

The total weight and volume of the unhardened CDR design are 2.18 kg (4.8 lbm) and 0.0026 m^3 (158 in.³), respectively. A breakdown of weight and volume allocations determined for each subassembly is presented in Table 21. As previously noted, 10 W-h of energy will be supplied from a self-contained battery.

5. Costs

In order to minimize development costs, the CDR design approach was based upon the use of proven techniques and state-of-the-art hardware. To this end the proposed transmitter is a commercially available unit and the foam-filled integral cavity-backed printed circuit spiral antenna is a design that has been developed and successfully tested by JPL under NASA advanced development sponsorship (Ref. 29). Similarly, the data encoder design utilizes presently available production line components that only require the application of suitable packaging techniques to meet the CDR design and functional requirements.

A developmental effort of approximately \$120K and of 6-months duration is contemplated followed by the production phase. A breakdown of development and production costs estimated for the unhardened CDR design is presented in Table 22. The \$15K production costs estimated for a unit of flight quality is based upon production lots of 50 to 100 units.

C. SENSORS AND SIGNAL PROCESSING

The sensors and their associated amplifiers are the same for the hardened and unhardened versions of the SMDI system. The output of each sensor is processed by an amplifier circuit to produce a standardized input to the data encoder.

Piezoelectric crystal types have extremely high source impedances that place severe constraints upon their connecting cables and amplifiers. Alternately, strain gauge types have low source impedances and can be used with normal cabling and amplifier techniques. Consequently, semiconductor strain gauges have been chosen as transducer elements in the accelerometers and pressure sensors of the SMDI.

The primary diagnostic instrument is a triaxial accelerometer. Its location is not critical as long as it can properly sense the motions of the spacecraft and interference with the telemetry subsystem. It will provide three channels of data. One is along the thrust-line with a range of measurement commensurate with the expected thrust, while two more-sensitive units are mounted transversely to measure lateral deflections. Miniature accelerometers of the strain gauge type with rated responses of 20 kHz are available. Qualitative indications considerably above this rate could be obtained.

It is believed that significant diagnostic information can be obtained by correlating triaxial acceleration with chamber pressure. Miniature strain gauge pressure sensors exist which can either be implanted internally beneath the motor insulation or operated remotely through a pressure port. The basic rated response of these instruments is 35 kHz.

Temperature at one or more locations will be determined by means of resistive temperature sensors. These sensors contain a small platinum element through which a constant current is passed. The resistance of the element, and hence the voltage developed across it by the constant current, is proportional to the temperature of the element. The output voltage is raised to a standardized level by the same type of amplifier as is used for the accelerometers and pressure sensors. The rated response-time of the temperature sensor is 0.5 s. Mounting is by bolting or bonding, depending upon the conditions at the chosen location.

The estimated weight, volume, and cost of a representative set of sensors and amplifiers are tabulated in Table 23. The additive increments to the properties estimated for the hardened and unhardened designs are 0.18 kg (0.40 lbm) and \$1.45K. Interconnecting cabling is estimated to further add ~ 0.113 kg (0.25 lbm) to the flight package. In an actual installation, the associated amplifiers are expected to be readily accommodated in that volume currently assigned to each candidate design.

D. COMPARISON OF CANDIDATE APPROACHES

Pertinent functional and design characteristics of the hardened and unhardened CDR designs are summarized in Tables 24 and 25. Each of the competing systems are unique in their diagnostic and performance capability and hence, a meaningful basis of comparing competing approaches is not readily apparent. The hardened design has the capability to fully meet the designated diagnostic and functional objectives under the severest environmental conditions anticipated. Design formulation is based upon an emphasis on telemetry performance margin utilizing low-rate digital and high-response data return. The hybrid approach provides complete diagnostic coverage in the form of general waveform, timed, untimed thresholded, and rate-sensitive data.

In addition, by incorporating the simultaneous radiation transmission option, the probability of a successful and complete retrieval of diagnostic data should approach unity regardless of the spacecraft condition, orientation, or environment. In view of the large performance margin established in Table 14, the obvious question arises as to whether the system proposed herein is over-designed. Clearly, numerous design tradeoffs could be exercised to reduce cost, power, weight, and size at the expense of additional mission risk and/or performance. Alternately, SMDI employment on missions beyond near-Earth applications (e.g., Surveyor) can be exploited. Thus, the key effort warranting attention during the initial development of the CDR involves a critical evaluation of the potential functional requirements in terms of their relative importance to representative sectors of the user community.

Although the unhardened design does not have the capability of surviving catastrophic failures wherein permanent CDR damage, spacecraft tumbling, etc., result, it should provide the minimum necessary diagnostic data in

real-time to suffice in the majority of cases. For the balance of incidents involving catastrophic failures, it should provide adequate data coverage up to the point of failure. The frequency response and overall performance of the alternate design will not be comparable to that provided by the hardened configuration; however, it may still be adequate to accomplish the bulk of required diagnostic functions.

The primary advantages of the unhardened design are; (1) minimal development costs (owing to the conventional telemetry system approach), (2) smaller production costs (~one third of the hardened system), and (3) lighter weight.

VII. CONCLUSIONS AND RECOMMENDATIONS

The following conclusions and recommendations were derived as a result of this study.

- (1) A need exists to incorporate added flight diagnostic instrumentation for future space flights employing solid rocket upper stages or apogee motors. This need arises because of the hierarchy of telemetry data that is assigned to the acquisition of competing spacecraft performance information which usually excludes in-flight diagnostic data from the solid motor.
- (2) The hardened SMDI system is recommended where a need exists to maximize the probability of a successful and complete retrieval of diagnostic data regardless of the character of the failure mode such as on deep space probes, space shuttle booster motors, sensitive military satellites, very costly commercial satellites, etc.
- (3) Alternately, where the primary need is for separate data acquisition/transmission, or where on-board data acquisition/transmission capability does not exist and cost is a consideration, the unhardened alternate system is recommended.

DEFINITION OF ABBREVIATIONS AND TERMS

ADC	Analog-to-digital converter
$AR_{s/c}$	Axial ratio of spacecraft (measure of the departure from circular polarization of spacecraft)
AR_g	Axial ratio of ground receiving station (measure of the departure from circular polarization of the spacecraft)
CDR	Critical data recorder
FM	Frequency modulation
FSK	Frequency shift keying
IRIG	Interrange instrumentation group
LPF	Low-pass filter
P_c	Chamber pressure
PM	Phase modulation
RF	Radio frequency
SMDI	Solid motor diagnostic instrumentation
T_0	Turn on
VCO	Voltage-controlled oscillator
VHF	Very high frequency

REFERENCES

1. Don, J. P., "System Effects on Motor Reliability Study - Interim Summary Report," IOM 385-72-177, Jet Propulsion Laboratory, Pasadena, Calif., Aug. 24, 1972 (JPL internal document).
2. McCaskill, A. M., and Cimino, A. A., "Failure Analysis and Environmental Testing of the Intelsat II Apogee Motor," AIAA Paper No. 68-246, presented at AIAA 2nd Flight Test, Simulation and Support Conference, Los Angeles, Calif., March 1968.
3. Gin, W., "Meeting of the Failure Review Team for COMSAT's Intelsat III F-8 Flight," IOM SM-381-70-93, July 31, 1970 (JPL internal document).
4. Private communications between E. M. Landsbaum of Aerospace Corporation and W. Gin of the Jet Propulsion Laboratory, Oct. 26, 1970.
5. Moseson, M. L., "Final Report of the Delta 71-73 Failure Review Committee," Goddard Space Flight Center, Greenbelt, Md., January 1970 (GSFC internal document).
6. Private communications between R. G. Urash of Vought Missile and Space Company, and J. P. Don of the Jet Propulsion Laboratory, May 16, 1972.
7. Ellion, M. E., et al., "Surveyor IV Propulsion Analysis Group Report," Report No. SSD 78132 R-1, Hughes Aircraft Company, El Segundo, Calif., Aug. 4, 1967.
8. King, M. W., "Rocket for Apogee Injection of a Hughes HS-303A Spacecraft," HAC-SSD Specification No. PS 30660-11, Rev. C, Hughes Aircraft Company, Culver City, Calif., Feb. 15, 1966.
9. Private communications on ground handling procedures between L. M. Spicer of Hughes Aircraft Company and Y. Nakamura of the Jet Propulsion Laboratory, April 1973.
10. Freeman, R. J., "Equipment Specification - Apogee Motor Intelsat III Satellite," TRW Specification No. EQ 8-30A, TRW Systems, Redondo Beach, Calif., Feb. 1, 1967.
11. Private communications between A. C. Ellings and K. Nall of TRW, Inc., and Y. Nakamura of the Jet Propulsion Laboratory, May 1973.
12. "Motor, Solid Propellant, Apogee Boost, Specification For," Specification No. SP-B01000D, Code 26463, Philco-Ford Corp., Newport Beach, Calif., October 1968.
13. Private communications between J. Hulbert and K. Sater of Philco-Ford Corp. and Y. Nakamura of the Jet Propulsion Laboratory, May 1973.

14. "Rocket Motor, Third Stage, Spherical Delta Space Research Vehicle DSV-3E," Contract Specification No. CP 00154, Revision No. B, McDonnell Douglas Corp., Dec. 18, 1967.
15. Private communications between E. M. Landsbaum of Aerospace Corporation and Y. Nakamura of the Jet Propulsion Laboratory, May 1973.
16. "Scout Planning Guide," Vought Missile and Space Company, Dallas, Texas, May 1971.
17. Private communications between S. Song of LTV and Y. Nakamura of the Jet Propulsion Laboratory, May 1973.
18. Private communications between J. Pletz of Thiokol Chemical Company and Y. Nakamura of the Jet Propulsion Laboratory, May 1973.
19. Don, J. P., and A. G. Piersol, "Systems Effects on the Reliability of Solid Propellant Rocket Motors," Document 900-622, July 26, 1973 (JPL internal document).
20. "Surveyor Spacecraft Functional Description," Pub. No. 65-96800, Rev. B, Hughes Aircraft Company, El Segundo, Calif., April 1, 1964.
21. "Mission Planners Guide to Burner II," Pub. No. D282601-5, second printing, The Boeing Company, Seattle, Wash., April 1968.
22. Norton, H. N., Handbook of Transducers for Electronic Measuring Systems, Prentice-Hall, Inc., New York, 1969.
23. Perino, P. R., "Characteristics of Thin Film Strain Gage Transducers," Preprint No. 16.11-3-66, 21st Annual Instrument Society of America Conference and Exhibit, New York, Oct. 24-27, 1966.
24. Private communications with Eph Konigsberg, Konigsberg Instruments, Inc., and W. S. Wuest of the Jet Propulsion Laboratory, Feb. 16, 1973.
25. Crawford, G. A., and Mazzocco, C. F., "Temperature Transducers and Measurements," Design File, VO'75-14-6. Jan. 26, 1972 (JPL internal document).
26. "Final Report, Failure-Warning System for Large Solid Motors," Report No. 0588-01F, Aerojet Solid Propulsion Company, Sacramento, Calif., April 1962.
27. "Final Report on Malfunction Warning System Study Program," Report No. 16-62, Thiokol, Huntsville, Ala., May 1962.
28. Adams, J. L., et al., "Critical Data Recorder Preliminary Design," Technical Memo 355-101, April 11, 1966 (JPL internal document).
29. Casani, E. K., "Capsule System Advanced Development Program Report," JPL Report 760-29, July 15, 1968 (JPL internal document).

Table 1. Findings of failure review board investigations

Motor/spacecraft	Motor burn time		Probable failure mode
	Anticipated, s	Actual, s	
Apogee motors			
SVM-1/Intelsat II, Flight 1	16	4.7 (Ref. 2)	Loss of nozzle assembly induced by low temperature excursion. Failure reproduced in ground test
SVM-2/Intelsat III H, Flight 8	27	14.5 ^a (Ref. 3)	Blow of motor or nozzle assembly due to motor case damage or defective nozzle
TE-M-521/Skynet II, Flight 2	21	13.9 (Ref. 4)	Motor case burnthrough due to thermal degradation of insulation
Upper stage motors			
TE-M-364-3/Intelsat III E, Flight 5	44	27 ^b (Ref. 5)	Thrust termination due to: (1) leakage at squib, igniter or nozzle closure, (2) nozzle closure failure, or (3) structural failure by premature release of yo weight
FW-4S/Orbiting Vehicle 3	32	17.3 (Ref. 6)	Inadequate nozzle throat design. Nozzle redesigned with high strength graphite and backup ring
Retro motor			
TE-364-1/Surveyor IV	40.7 to 42.7	31.1 ^a (Ref. 7)	Cause unknown. If retro motor at fault possibly due to liner-insulation separation failure
^a Telemetry data lost			
^b Inferred from telemetry data			

Table 2. Storage and transportation data

Motor (Spacecraft)	Requirements					Rejection criteria	Anomalies during lifetime
	Time, mo	Temperature, K	Percent of humidity	Vibration	Shock		
SVM-1 (Intelsat II, Flight 1)	12 (Ref. 8)	272 to 317 294 \pm 5.6 during transportation, 297 \pm 2.8 during storage (Ref. 8)	< 50 during transportation, < 65 during storage (Ref. 8)	Not stated (air-ride van transported) (Ref. 8)	< 3 g (Ref. 8)	\geq 5 g shock; visual and cold X-ray examination for damage or degra- dation (Ref. 9)	Low tempera- ture excursion in space prior to motor ignition (Ref. 8)
SVM-2 (Intelsat III H, Flight 8)	36 (Ref. 10)	267 to 323 (Ref. 10)	< 65 (98%, 306 K, 120 h) (Ref. 10)	Not stated (Ref. 10)	65.6-m drop to steel faced concrete in shipping con- tainer (Ref. 10)	If container shows damage, motor undergoes visual and X-ray inspec- tion. X-ray exami- nation prior to assembly at the launch site (Ref. 11)	Uncontrolled temperature environment for 12 months (Ref. 10)
TE-M-521 (Skynet II, Flight 2)	24 (Ref. 12)	256 to 317 (244 and 339, 8 h) (Ref. 12)	100; no time stated (Ref. 12)	Not stated (Ref. 12)	With motor in ship- ping container: (a) half sine, 15-g peak, 11 ms, 3 per direction; (b) using one end as pivot, lift other end 10.2 cm and drop to wooden bench top, 4 per face (Ref. 12)	Visual and X-ray examination for damage and degra- dation (Ref. 13)	Storage time in excess of procurement specification requirements (29 months) (Ref. 12)
TE-M-364-3 (Intelsat III E, Flight 5)	24 (Ref. 4)	278 to 311 (Ref. 14)	< 50 (95%, 311 K, 42 h) (Ref. 14)	1.3 g; 2.54 cm double amplitude displace- ment 1-5 Hz; roll off double-amplitude displacement from 2.54 cm to 0.091 cm from 5 to 26 Hz; 0.091-cm double- amplitude displace- ment from 26 to 52 Hz (Ref. 14)	Supporting one end 15.2 cm above ground, drop other end from height of 61 cm to concrete, 1 per edge (motor in shipping con- tainer) (Ref. 14)	If shipping container shows evidence of damage, motor is examined by visual, ultrasonic, and radiographic inspec- tion (Ref. 15)	Motor dropped in container shortly after arrival at KSC, considered insignificant (Ref. 14)
FW-4S (Orbiting Vehicle 3)	12 (Ref. 16)	272 to 317 (Ref. 16)	< 60 (Ref. 16)	Not stated (Ref. 16)	Not stated (Ref. 16)	Visual and radio- graphic inspection for separation defect or voids. Exceedance of qualification con- straints (Ref. 17)	Excessive storage life ($<$ 24 months) (Ref. 16)
TE-364-1 (Surveyor IV)	< 24 (Ref. 18)	267 to 317 (Ref. 18)	3 to 95 (Ref. 18)	Not stated (Ref. 18)	Two 45.7-cm vertical drop tests on to concrete pad (nozzle up in ship- ping container) (Ref. 18)	Visual and cold radiographic inspection (Ref. 18)	No unusual liens noted (Ref. 18)

Table 3. Representative monitoring and surveillance practices

Solid motor measurement	Type of coverage	Sampling rate, sample/sec
Surveyor spacecraft		
Retro acceleration	Commutated	4
Retro case strain gauge	Commutated	1
Lower retro case temperature	Commutated	1
Upper retro case temperature	Commutated	1
Retro nozzle temperature	Commutated	1
Burner II		
Accelerometer	Continuous	—
Pressure transducer	Commutated	10

Table 4. Typical available instruments

Measurement	Chamber pressure gauge Bell & Howell (CEC) 4-356-0003	Chamber pressure gauge Endevco 2501	Chamber pressure gauge Konigsberg Inst. P14E	Accelerometer Endevco 2228	Accelerometer Konigsberg Inst. A-3	Temperature gauge Rosemount Eng.
Range	0 to 6.89×10^6 N m ⁻² (0 to 1000 psi)	0 to 6.89×10^6 N m ⁻² (0 to 1000 psi)	0 to 6.89×10^6 N m ⁻² (0 to 1000 psi)	±10 g	±10 g	13 to 1073 K
Natural frequency, kHz	50	50	175	24	100	—
Rated response	1 kHz	10 kHz	35 kHz	4 kHz	20 kHz	0.5 s
Accuracy, %	±0.25	±3	±0.5	2.5	±1.0	±0.1
Thermal sensitivity shift	0.009%/K	—	0.009%/K	—	±0.5% full-scale/K	—
Resolution	Infinite	Infinite	—	—	—	Infinite
Construction	Strain gauge	Crystal	Strain gauge	Crystal	Strain gauge	Pt wire
Weight, g	71	20	0.5	15.3	0.53	1 to 10
Cost, \$	675	200	150	525	500	100

Table 5. Solid motor diagnostic instrumentation characteristics

Signal/instrument ^a	Range	Accuracy	Resolution	Frequency response	Waveform
3-Axis accelerometer	0 to 20 g (lateral axis)	$\begin{cases} \leq \pm 1\% \\ \text{desirable} \end{cases}$	$\begin{cases} < \pm 1\% \\ \text{desirable} \end{cases}$	≥ 2 kHz	Exponential
	0 to 2 g (orthogonal axes)	$\begin{cases} \leq \pm 5\% \\ \text{acceptable} \end{cases}$	$\begin{cases} < \pm 5\% \\ \text{acceptable} \end{cases}$		
Chamber pressure	Vacuum to 6.89×10^6 N m ⁻²	$\begin{cases} \leq \pm 1\% \\ \text{desirable} \end{cases}$	$\begin{cases} < \pm 1\% \\ \text{desirable} \end{cases}$	≥ 5 kHz	Exponential
	(Vacuum to 1000 psia)	$\begin{cases} \pm 5\% \\ \text{acceptable} \end{cases}$	$\begin{cases} < \pm 5\% \\ \text{acceptable} \end{cases}$		
Temperature	255-316 K (0 to 110°F) prefire, 644 K (700°F) maximum postignition	$\leq \pm 5\%$	$< \pm 5\%$	≥ 1 Hz	Exponential

^aAll instruments with zero overshoot

Table 6. Thresholded data system requirements

Parameter	Typical trace	Functional requirements
Temperature (2 probes)		<p>Interrogate and time-tag three events up within normal operational range</p> <p>Time-tag one event up and down to detect anomalies for out-of-spec measurements</p> <p>Untimed events are desirable to monitor temperature in pre- and post-ignition states (in finer increments) within normal operational regime</p>
Chamber pressure		<p>Interrogate and time-tag only those events necessary to detect anomalies</p> <p>Two time-tagged events up and down within nominal range to establish burn duration and rise time</p> <p>Two time-tagged events above normal P_c range</p> <p>Additional untimed measurements required to yield performance data in finer increments within nominal operational range</p> <p>Detect frequency and amplitude of combustion instabilities</p>
Accelerometer (3 axes)		<p>Interrogate and time-tag only those events necessary to detect anomalies</p> <p>Two time-tagged events up and one down in normal range of operation to determine rise and fall times in axial (thrust axis) and each orthogonal accelerometer</p> <p>Two time-tagged events above normal lateral g loading range to detect anomalies</p> <p>One time-tagged event above normal g loading range to detect anomalies in orthogonal accelerometers</p> <p>Untimed events required to detect performance output (in finer increments) within normal operational range</p> <p>Steady-state readout (untimed) desirable but not mandatory</p> <p>Detect frequency and amplitude of g level oscillations in each orthogonal accelerometer</p>
T = temperature t = time	P_c = chamber pressure g = thrust axis acceleration	g' = orthogonal axis acceleration X_{t_i} = time-tagged event

Table 7. Failure modes and effects summary for real-time system^a

Primary failure mode	Cause of failure	Effects	Telemetry signature	Remarks
Blow of motor	Overpressurization, thermal overheating, case strength failure, environment, micro-meteorite impact	Loss of communications, violent spacecraft motion, abnormal chamber pressure, change in altitude, insufficient ΔV	Partial or complete loss of data, disturbing torques, momentary P_c and acceleration spikes, unplanned telemetry doppler shift, gyro shift	Can occur at any time during the burn. Statistics indicate 29% of all catastrophic failures occur within 1 s and 51.5% occur within 10 s of stage ignition. Less than 1% of motors explode with no prior indication of malfunction
Nozzle failure modes Nozzle blowout	Improper design, manufacturing error, sport ^b , case limit exceedance, environment	Insufficient ΔV , high heat input to motor case, large coning angle, thrust peak and low continuation, abnormal chamber pressure (rapid pressure rise and rupture in the event of nozzle blockage)	Disturbing torques, abnormal P_c , change in altitude, unplanned telemetry doppler shift, g signal peak and decay, abnormal temperature rise, sun angle change	Nozzle failures tend to occur late in burn, assuming ignition phase is passed
Nozzle failure	Thermal and shock loading excursions, structural defects, processing defects, damage during ground handling, environment (orbit temperature cycling)			
Case burnthrough	Grain deficiencies, insulation breakdown, hot gas leak, installation error, combustion product slag	Abnormal motor/spacecraft heating, change in altitude, large coning angle, catastrophic failure preceded by reduced thrust	Abnormal temperature rise, disturbing torques, anomalous P_c traces, unplanned telemetry doppler shift, sun angle change, abnormal and/or oscillating traces on transverse accelerometer(s)	Case burnthroughs recorded at any time from 10 to 90% of web burn. In the event of burnthrough, ~ 1 s will elapse before structural failure and, during this interval, a significant change in axial thrust will occur. Case burnthrough can result in violent rupture with no abnormal rise in pressure prior to failure or burn as long as several seconds after burnthrough before exploding
Failure or interruption of ignition	Failure to ignite, blows, S&A ejection, structural failure, installation error, environment, loss of aft closure	ΔV discrepancies, change in altitude, thrust termination	Loss or absence of P_c , abnormal temperature trace, unplanned telemetry doppler shift, anomalous thrust signal	If ignition is terminated by catastrophic failure, the same remarks associated with blow of motor apply
Combustion instability	Improper design, propellant, or motor dynamic response characteristics	Violent spacecraft motion, abnormal chamber pressure, high frequency thrust variations and possible case burnthrough resulting in spacecraft tumbling	High-oscillation P_c trace, disturbing torques, unplanned telemetry doppler shift, sun angle change, high temperature readings, possible abnormal gyro error and thrust command signals	Can occur at any time during the burn. May result in catastrophic failure of motor

^aRefs. 7, 26, and 27^bAnomaly that lies outside of sampled population

Table 8. Failure mode detection and discrimination for thresholded system

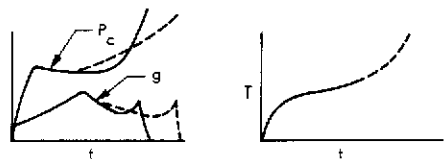
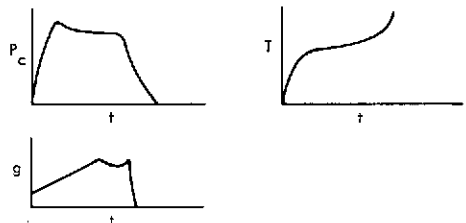
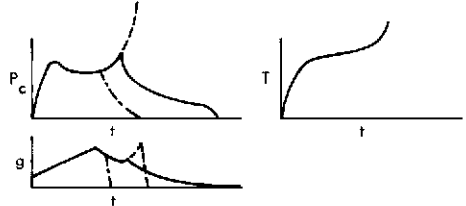
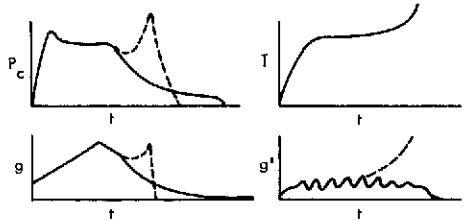
Primary failure mode	Typical diagnostic trace	SMDI detection	Ground/spacecraft discrimination
Blow of motor Case rupture		Exceedance of 2 overpressure and g level (multi-axes) threshold indicators for catastrophic failure. May be preceded by slow increase in P_c and g traces. Abrupt loss of signals	Partial or complete loss of data, unplanned telemetry doppler shift, gyro shift, change in altitude
Nozzle failure modes Nozzle blowout		Abrupt loss in P_c with rapid decay. Exceedance of one or more g level threshold indicators (longitudinal) accompanied by rapid decay. Premature detection of low level threshold indicators (termination for both P_c and g traces)	Unplanned telemetry doppler shift, sun angle change, change in altitude, insufficient ΔV , large coning angle
Nozzle failure		P_c and g level peak and decay (abnormally long duration). Rapid pressure rise and case rupture in the event of nozzle blockage. Possible exceedance of one or more P_c and g high level trips. Abnormal temperature rise. Sudden loss and decay of P_c and g traces	
Case burnthrough		Abnormal temperature rise. High frequency and/or amplitude g loading in transverse axes. Anomalous duration in P_c and g traces. Catastrophic failure possibly preceded by reduced P_c and g levels (actuation of one or more overage thresholds and one termination trip). Abrupt loss of signals	Large coning angle, sun angle change, unplanned telemetry doppler shift, change in altitude, abnormal spacecraft heating

Table 8. (contd)

Primary failure mode	Typical diagnostic trace	SMDI detection	Ground/spacecraft discrimination
Failure or interruption of ignition		Loss or absence of P_c and g level readings (abnormal duration). Anomalous temperature trace. (Timed and untimed events available to discern profile and histogram)	Unplanned telemetry doppler shift, change in altitude
Combustion instability		High frequency (~200 to 1700 Hz) and amplitude (1 to 20%) oscillations on P_c trace. May lead to case rupture and actuation of high-level P_c and g indicators. Low-frequency instability may lead to incomplete combustion, premature extinguishment, and deterioration of performance	Unplanned telemetry doppler shift, sun angle change, change in altitude, insufficient ΔV

Table 9. CDR timed events

Event		Event ID
1. > 0.1 g ^a	x-Axis accel.	0 0 0 0 1
2. > 0.2 g	x-Axis accel.	0 0 0 1 0
3. > 2.0 g	x-Axis accel.	0 0 0 1 1
4. < 0.1 g	x-Axis accel.	0 0 1 0 0
5. > 0.1 g	y-Axis accel.	0 0 1 0 1
6. > 0.2 g	y-Axis accel.	0 0 1 1 0
7. > 2.0 g	y-Axis accel.	0 0 1 1 1
8. < 0.1 g	y-Axis accel.	0 1 0 0 0
9. > 1.0 g	z-Axis accel.	0 1 0 0 1
10. > 2.0 g	z-Axis accel.	0 1 0 1 0
11. > 8.0 g	z-Axis accel.	0 1 0 1 1
12. > 10.0 g	z-Axis accel.	0 1 1 0 0
13. < 1 g	z-Axis accel.	0 1 1 0 1
14. > $3.45 \times 10^5 \text{ Nm}^{-2}$ (50 psia)	Press. transducer	0 1 1 1 0
15. > $2.65 \times 10^6 \text{ Nm}^{-2}$ (300 psia)	Press. transducer	0 1 1 1 1
16. > $4.83 \times 10^6 \text{ Nm}^{-2}$ (700 psia)	Press. transducer	1 0 0 0 0
17. > $6.89 \times 10^6 \text{ Nm}^{-2}$ (1000 psia)	Press. transducer	1 0 0 0 1
18. < $3.45 \times 10^5 \text{ Nm}^{-2}$ (50 psia)	Press. transducer	1 0 0 1 0
19. > 255 K (0°F)	Temp. 1	1 0 0 1 1
20. > 310 K (100°F)	Temp. 1	1 0 1 0 0
21. > 366 K (200°F)	Temp. 1	1 0 1 0 1
22. > 644 K (700°F)	Temp. 1	1 0 1 1 0
23. > 255 K (0°F)	Temp. 2	1 0 1 1 1
24. > 310 K (100°F)	Temp. 2	1 1 0 0 0
25. > 366 K (200°F)	Temp. 2	1 1 0 0 1
26. > 644 K (700°F)	Temp. 2	1 1 0 1 0
27. Oscillatory event ^b	Press. transducer	1 1 0 1 1
28. Oscillatory event ^b	y-Axis accel.	1 1 1 0 0
29. Oscillatory event ^b	z-Axis accel.	1 1 1 0 1

^aThe thresholds shown were selected as being representative and may be adjusted to any preselected value appropriate for a given mission.

^bIncludes occurrence, frequency, and amplitude information.

Table 10. CDR nontimed events

1. > 0.01 g ^a	x-Axis accel.	27. < $6.89 \times 10^3 \text{ Nm}^{-2}$	Press. transducer
2. > 0.05 g	x-Axis accel.	28. < $6.89 \times 10^4 \text{ Nm}^{-2}$	Press. transducer
3. > 0.1 g	x-Axis accel.	29. < $1.03 \times 10^5 \text{ Nm}^{-2}$	Press. transducer
4. > 0.2 g	x-Axis accel.	30. > $3.45 \times 10^5 \text{ Nm}^{-2}$	Press. transducer
5. > 0.5 g	x-Axis accel.	31. > $1.38 \times 10^6 \text{ Nm}^{-2}$	Press. transducer
6. > 0.7 g	x-Axis accel.	32. > $2.65 \times 10^6 \text{ Nm}^{-2}$	Press. transducer
7. > 1.0 g	x-Axis accel.	33. > $2.76 \times 10^6 \text{ Nm}^{-2}$	Press. transducer
8. > 2.0 g	x-Axis accel.	34. > $3.45 \times 10^6 \text{ Nm}^{-2}$	Press. transducer
9. > 0.01 g	y-Axis accel.	35. > $4.14 \times 10^6 \text{ Nm}^{-2}$	Press. transducer
10. > 0.05 g	y-Axis accel.	36. > $4.83 \times 10^6 \text{ Nm}^{-2}$	Press. transducer
11. > 0.1 g	y-Axis accel.	37. > $6.89 \times 10^6 \text{ Nm}^{-2}$	Press. transducer
12. > 0.2 g	y-Axis accel.	38. > 255 K	Temp. gauge 1
13. > 0.5 g	y-Axis accel.	39. > 278 K	Temp. gauge 1
14. > 0.7 g	y-Axis accel.	40. > 295 K	Temp. gauge 1
15. > 1.0 g	y-Axis accel.	41. > 310 K	Temp. gauge 1
16. > 2.0 g	y-Axis accel.	42. > 366 K	Temp. gauge 1
17. > 1.0 g	z-Axis accel.	43. > 479 K	Temp. gauge 1
18. > 2.0 g	z-Axis accel.	44. > 644 K	Temp. gauge 1
19. > 3.0 g	z-Axis accel.	45. > 255 K	Temp. gauge 2
20. > 4.0 g	z-Axis accel.	46. > 278 K	Temp. gauge 2
21. > 5.0 g	z-Axis accel.	47. > 295 K	Temp. gauge 2
22. > 6.0 g	z-Axis accel.	48. > 310 K	Temp. gauge 2
23. > 7.0 g	z-Axis accel.	49. > 366 K	Temp. gauge 2
24. > 8.0 g	z-Axis accel.	50. > 479 K	Temp. gauge 2
25. > 9.0 g	z-Axis accel.	51. > 644 K	Temp. gauge 2
26. > 10.0 g	z-Axis accel.		

^aThe thresholds shown were selected as being representative and may be adjusted to any preselected value appropriate for a given mission.

Table 11. Spacecraft radio transmission parameters – hardened design

Parameter	Capsule-mounted antenna system	
	Design value	Uncertainty tolerance, dB
Total transmitter power ^a	+23.0 dBmW	+0.0 -1.0
Carrier modulation loss ^b	-5.4 dB	+1.2 -1.5
Transmitting circuit loss ^c	-2.5 dB	±0.9
Spacecraft antenna gain ^d	+5.3 dB ^e	±0.5
Impact degradation loss ^f	Unknown	Unknown
Spacecraft antenna pointing loss	-5.8 dB	±1.0

^a0.2 W at the output of the final multiplier.

^bBased upon carrier modulation of 1.45 ± 10 percent rad peak.

^cIncludes all circuitry between the output of the final multiplier and the input to the antenna.

^dReference to perfectly circular isotropic, pattern maximum.

^eIncludes loss in impact limiting radome and reflects loss due to interference via antenna switch leakage.

^fPerformance estimates, parameters or tolerances do not include degradation due to antenna damage.

Table 12. Radio reception parameters — hardened design

Parameter	Value	Tolerance
Antenna gain ^a	+44.0 dB	+1.0 dB -0.5 dB
Circuit loss ^b	-0.2 dB	±0.1 dB
Effective system noise temperature ^c	165 K	±10 K
Receiver noise spectral density	-176.4 dBmW/Hz	+0.1 dB -0.3 dB
Carrier APC noise bandwidth ($2B_{Lo} = 48$ Hz)	+16.8 dB, Hz	+0.0 dB -0.4 dB
Carrier threshold SNR in $2B_{Lo}$	+6.0 dB	—

^aBased on 9.1 m (30-ft-diam) IRIG station antenna

^bCircuit loss includes diplexer, switch, and wave guide losses

^cIncludes contributions due to antenna temperature, circuit losses, low noise amplifier, and follow-on receiver

Table 13. Telemetry parameters — hardened design

Type of encoding	Digital frequency shift keying
Transmission rate	4 bits/s
Bit error probability at threshold	5×10^{-3}
Subcarrier noise bandwidth at threshold	+14.3 dB, Hz $\begin{matrix} +0.4 \\ -0.5 \end{matrix}$ dB
Required SNR for bit error probability of 5×10^{-3}	+5.6 dB
Data subcarrier modulation loss	-2.2 $\begin{matrix} +0.3 \\ -0.5 \end{matrix}$ dB

Table 14. Telecommunications link design control table —
hardened design

Parameter	Design value	Uncertainty tolerance, dB
Total transmitter power 0.2 W	+23.0 dBmW	+0.0 -1.0
Transmitting circuit loss	-2.5 dB	±0.9
Transmitting antenna gain	+5.3 dB	±0.5
Transmitting antenna pointing loss	-5.8 dB	±1.0
Space loss at 2290.2 MHz, range = 4.02×10^4 km	-191.8 dB	—
Polarization loss	-0.0 dB	±0.1
AR _{s/c} 2.5 dB		
AR _g 0.7 dB		
Receiving antenna gain	+44.0 dB	+1.0 -0.5
Receiving antenna pointing loss	—	—
Receiving circuit loss	-0.2 dB	±0.1
Net circuit loss	-151.0 dB	+3.6 -3.1
Total received power	-128.0 dBmW	+3.6 -4.1
Receiver noise spectral density (noise to bandwidth ratio)	-176.4 dBmW/Hz	+0.1 -0.3
T system = 165 ±10 K		
Carrier modulation loss	-5.4 dB	+1.2 -1.5
Received carrier power	-133.4 dBmW	+4.8 -5.6
Carrier APC noise bandwidth ($2B_{Lo} = 48$ Hz)	+16.8 dB, Hz	+0.0 -0.4
Threshold carrier SNR in $2B_{Lo}$	+6.0 dB	—
Threshold carrier power	-153.6 dBmW	+0.1 -0.7
Carrier performance margin	+20.2 dB	+4.9 -6.3
Subcarrier modulation loss	-2.2 dB	+0.3 -0.5
Received subcarrier power	-130.2 dBmW	+3.9 -4.6
Subcarrier noise bandwidth (noise bandwidth = 26.8 Hz) bit rate = 4.0 bits/s	+14.3 dB, Hz	+0.4 -0.5
Threshold subcarrier SNR in noise bandwidth	+5.6 dB	—
Threshold subcarrier power	-156.5 dBmW	+0.5 -0.8
Subcarrier performance margin	+26.3 dB	+4.4 -5.4

Table 15. CDR weight and volume breakdown — hardened design

Subassembly/element	Volume, m^3 (in. ³)	Weight, kg (lbm)
Upper antenna cap subassembly	0.00377 (230)	1.45 (3.2)
Transmitter/battery subassembly	0.00152 (93)	1.59 (3.5)
Data encoder subassembly	0.00095 (58)	0.68 (1.5)
Lower antenna cap subassembly	0.00134 (82)	0.45 (1.0)
Impact limiter	0.00211 (129)	0.50 (1.1)
Totals	0.00969 (592)	4.67 (10.3)

Table 16. CDR cost summary -- hardened design

Development costs	
Detailed design (includes drawings)	120K
Breadboard (fabrication and test)	40K
Prototype (fabrication and test)	60K
Documentation (reports and test procedures)	20K
Total	\$240K
Production costs (lots of 50 to 100 units)	
Transmitter/battery subassembly	20K
Battery	2K
Data encoder subassembly	8K
Upper antenna cap assembly	7K
Lower antenna cap subassembly	3K
Integration and test	5K
Total	\$45K

Table 17. Spacecraft radio transmission parameters –
unhardened design

Parameter	Capsule-mounted antenna system	
	Value	Tolerance, dB
Total transmitter power ^a	+40.0 dBmW	+0.0 -1.0
Carrier modulation loss ^b	-5.4 dB	+1.2 -1.5
Transmitting circuit loss ^c	-2.5 dB	±0.9
Spacecraft antenna gain ^d	+5.3 dB	±0.5
Spacecraft antenna pointing loss	-5.8 dB	±1.0

^a10 W at the output of the final multiplier

^bBased upon carrier modulation of $1.45 \pm 10\%$ rad peak

^cIncludes all circuitry between the output of the final multiplier and the input to the antenna

^dReference to perfectly circular isotropic, pattern maximum

Table 18. Radio reception parameters — unhardened design

Parameter	Value	Tolerance, dB
Antenna gain ^a	+44.0 dB	+1.0 -0.5
Circuit loss ^b	-0.2 dB	±0.1
Effective system noise temperature ^c	165 K	±10 K
Receiver noise spectral density	-176.4 dBmW/Hz	+0.1 -0.3
Carrier APC noise bandwidth ($2B_{Lo} = 48$ Hz)	+16.8 dB, Hz	+0.0 -0.4
Carrier threshold SNR in $2B_{Lo}$	+6.0 dB	—

^aBased on 9.1 m (30-ft-diam) IRIG station antenna

^bCircuit loss includes diplexer and waveguide losses

^cIncludes contributions due to antenna temperature, circuit losses, low-noise amplifier, and follow-on receiver

Table 19. Telemetry parameters — unhardened design

Type of encoding	FM/PM
Subcarrier noise bandwidth at threshold (69 kHz)	+48.4 dB, Hz $\begin{matrix} +0.4 \\ -0.5 \end{matrix}$ dB
Threshold subcarrier SNR in noise bandwidth	+9 dB
Data subcarrier modulation loss	-2.2 dB $\begin{matrix} +0.3 \\ -0.5 \end{matrix}$ dB

Table 20. Telecommunications link design control table —
unhardened design

Parameter	Design value	Uncertainty tolerance, dB
Total transmitter power 10 W	+40.0 dBmW	+0.0 -1.0
Transmitting circuit loss	-2.5 dB	±0.9
Transmitting antenna gain	+5.3 dB	±0.5
Transmitting antenna pointing loss	-5.8 dB	±1.0
Space loss	-191.8 dB	—
at 2290.2 MHz, Range = 4.02×10^4 km		
Polarization loss	-0.0 dB	±0.1
AR _{s/c} 2.5 AR _g 0.7 dB		
Receiving antenna gain	+44.0 dB	+1.0 -0.5
Receiving antenna pointing loss	—	
Receiving circuit loss	-0.2 dB	±0.1
Net circuit loss	-151.0 dB	+3.6 -3.1
Total received power	-111.0 dBmW	+3.6 -4.1
Receiver noise spectral density (noise-to-bandwidth ratio)	-176.4 dBmW/Hz	+0.1 -0.3
T system = 165 ±10 K		
Carrier modulation loss	-5.4 dB	+1.2 -1.5
Received carrier power	-116.4 dBmW	+4.8 -5.6
Carrier APC noise bandwidth ($2B_{Lo} = 48$ Hz)	+16.8 dB, Hz	+0.0 -0.4
Threshold carrier SNR in $2B_{Lo}$	+6.0 dB	—
Threshold carrier power	-153.6 dBmW	+0.1 -0.7
Carrier performance margin	+37.2 dB	+4.9 -6.3
Subcarrier modulation loss	-2.2 dB	+0.3 -0.5
Received subcarrier power	-113.2 dBmW	+3.9 -4.6
Subcarrier noise bandwidth (69 kHz)	+48.4 dB, Hz	+0.4 -0.5
Threshold subcarrier SNR in noise bandwidth	+9 dB	—
Threshold subcarrier power	-119.0 dBmW	+0.5 -0.8
Subcarrier performance margin	+5.8 dB	+4.4 -5.4

Table 21. Unhardened CDR design weight and volume breakdown

Subassembly/element	Volume, m ³ (in. ³)	Weight, kg (lbm)
Antenna cap subassembly	0.00098 (60)	0.454 (1.0)
Data encoder/radio/power subassembly		
Data encoder	0.00012 (7)	0.136 (0.3)
Radio	0.00026 (16)	0.454 (1.0)
Power	0.00036 (22)	0.544 (1.2)
Subchassis metal	0.00030 (18)	0.590 (1.3)
Unused space	0.00057 (35)	—
Subtotal	0.00161 (98)	1.724 (3.8)
Total	0.00259 (158)	2.178 (4.8)

Table 22. Unhardened CDR design cost summary

Development costs	
Detailed design	60K
Breadboard fabrication and test	20K
Prototype fabrication and test	30K
Documentation (reports and test procedures)	<u>10K</u>
Total	\$120K
Production costs ^a	
Data encoder/radio/power subassembly	10K
Antenna cap subassembly	3K
Integration and test	<u>2K</u>
Total	\$15K
^a Production lots of 50 to 100 units	

Table 23. Typical sensor and amplifier package

Component	Manufacturer or Description	Weight, kg (lbm)	Volume m ³ (in. ³)	Cost, \$K
Triaxial accelerometer	Konigsberg Instruments, Inc. (A3)	0.027 (0.06)	0.000016 (1.0)	0.50
Pressure sensor	Konigsberg Instruments, Inc. (P14E)	0.054 (0.12)	0.000013 (0.8)	0.15
Temperature sensor (2 each)	Rosemount Engineering	0.009 (0.02)	0.000003 (0.2)	0.20
Amplifiers (6 each)	6 A	0.091 (0.20)	0.000066 (4.0)	0.60
Totals		0.181 (0.40)	0.000098 (6.0)	1.45

Table 24. Summary of functional and unit characteristics of candidate designs

Design	Telemetry	Environmental	Data characteristics	Advantages
Hardened	Both real and nonreal-time coverage	Hardened for 10,000 g	High response digital data	Complete diagnostic coverage under all conditions
	Large telemetry performance margin		General waveform information	
			Timed and untimed thresholded data	
			Rate-sensitive data	
Unhardened	Only real-time coverage	Unhardened package	Limited frequency response	Smaller Lighter Reduced cost

Table 25. Summary of SMDI candidate design properties

Item	Target value	Hardened design	Unhardened design
Weight	$\leq 5.44 \text{ kg (12 lbm)}$	4.94 kg (10.9 lbm)	2.45 kg (5.4 lbm)
Volume	$\leq 0.014 \text{ m}^3 (0.5 \text{ ft}^3)$	$0.0097 \text{ m}^3 (0.34 \text{ ft}^3)$	$0.0026 \text{ m}^3 (0.09 \text{ ft}^3)$
Development costs		\$240K	\$120K
Flight unit costs	$\leq \$50\text{K}$ (~\$20K desirable)	\$46.5K ^a	\$16.5K ^a
^a Production lots of 50 to 100 units			

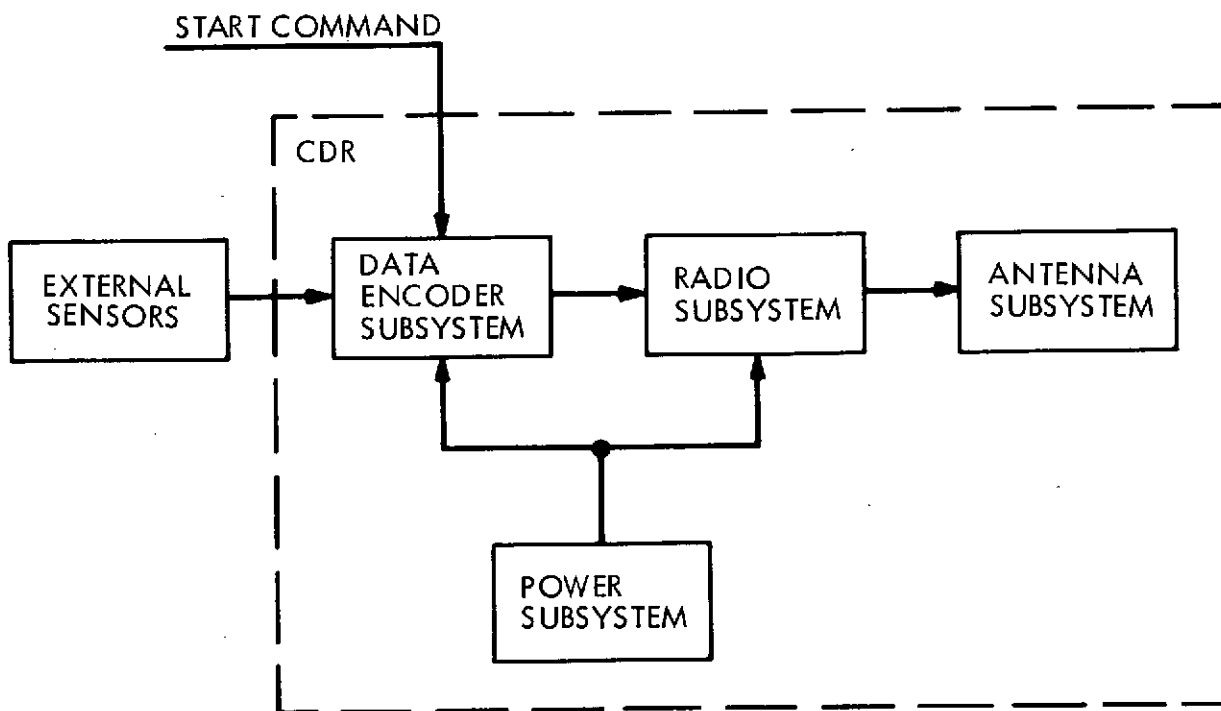
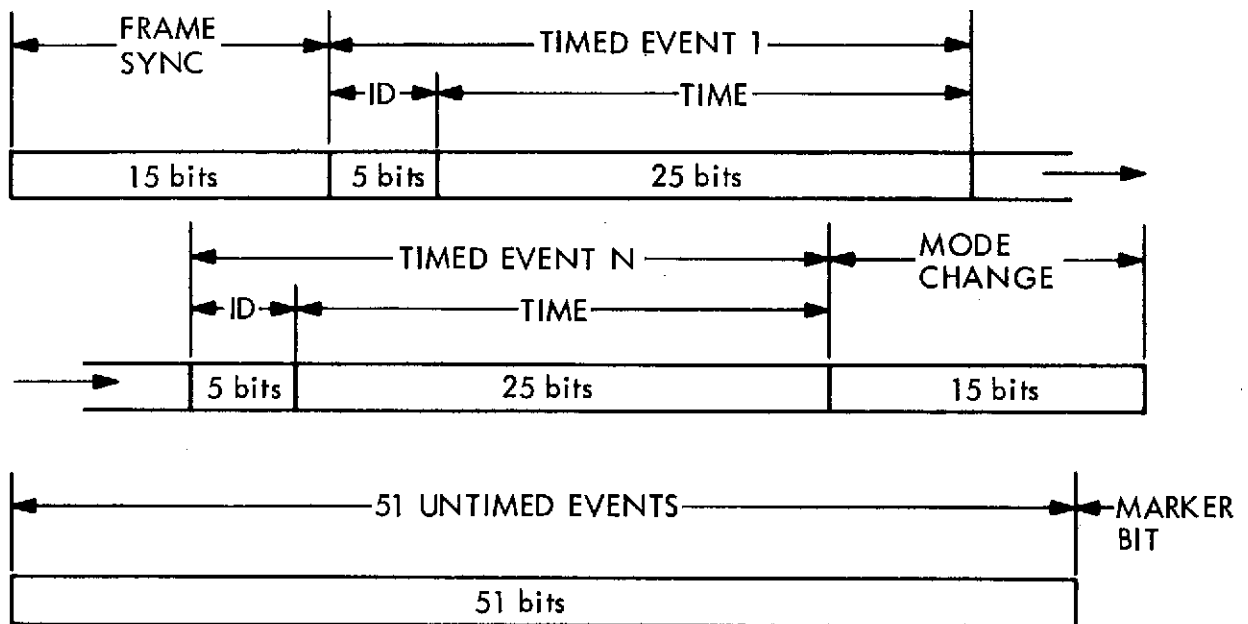


Fig. 1. SMDI system block diagram



FRAME LENGTH

ID	=	30 bits	FRAME TIME = 1305 bits ÷ 4 bits/s
TIMED EVENTS	=	1224 bits MAX	= 326.25 s MAX
UNTIMED EVENTS	=	51 bits	
TOTAL	=	1305 bits MAX	

Fig. 2. Typical CDR data frame

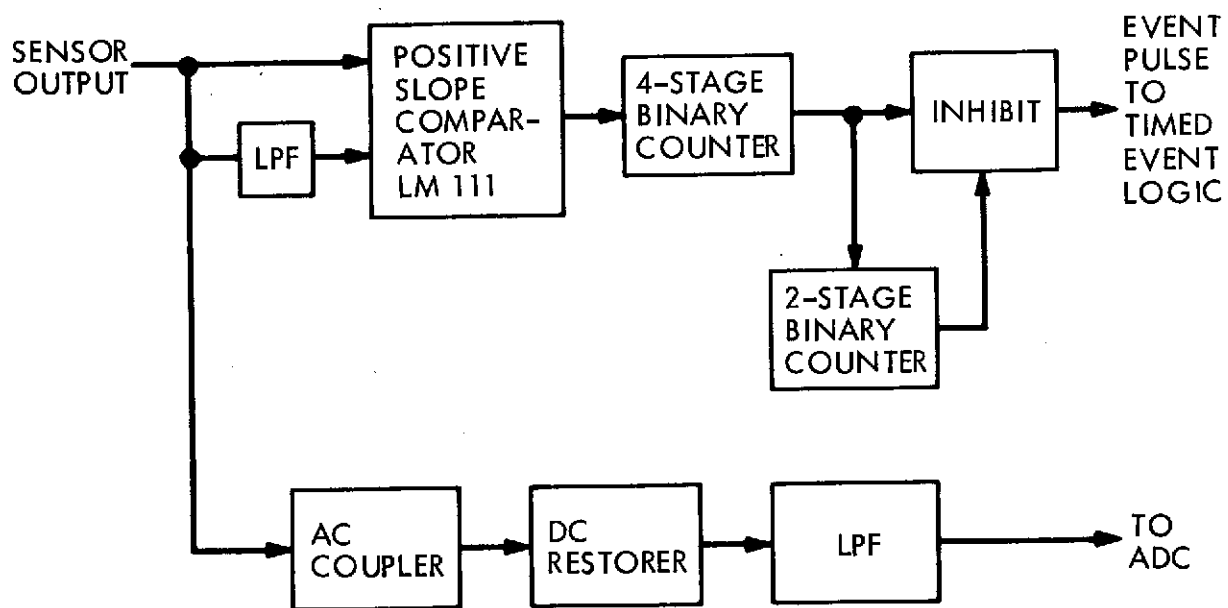


Fig. 3. Oscillatory event detection circuitry

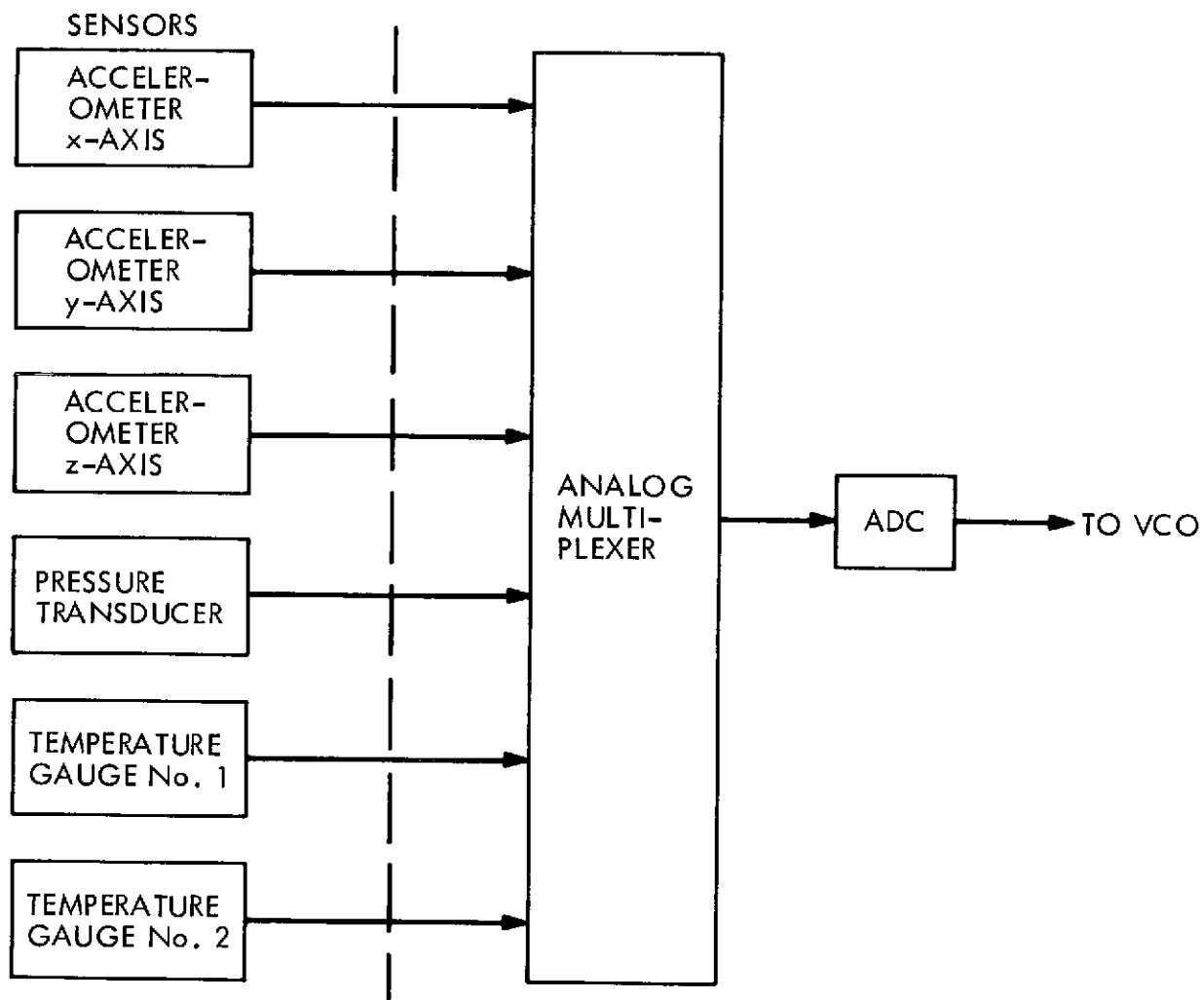


Fig. 4. CDR data encoder real-time data processing

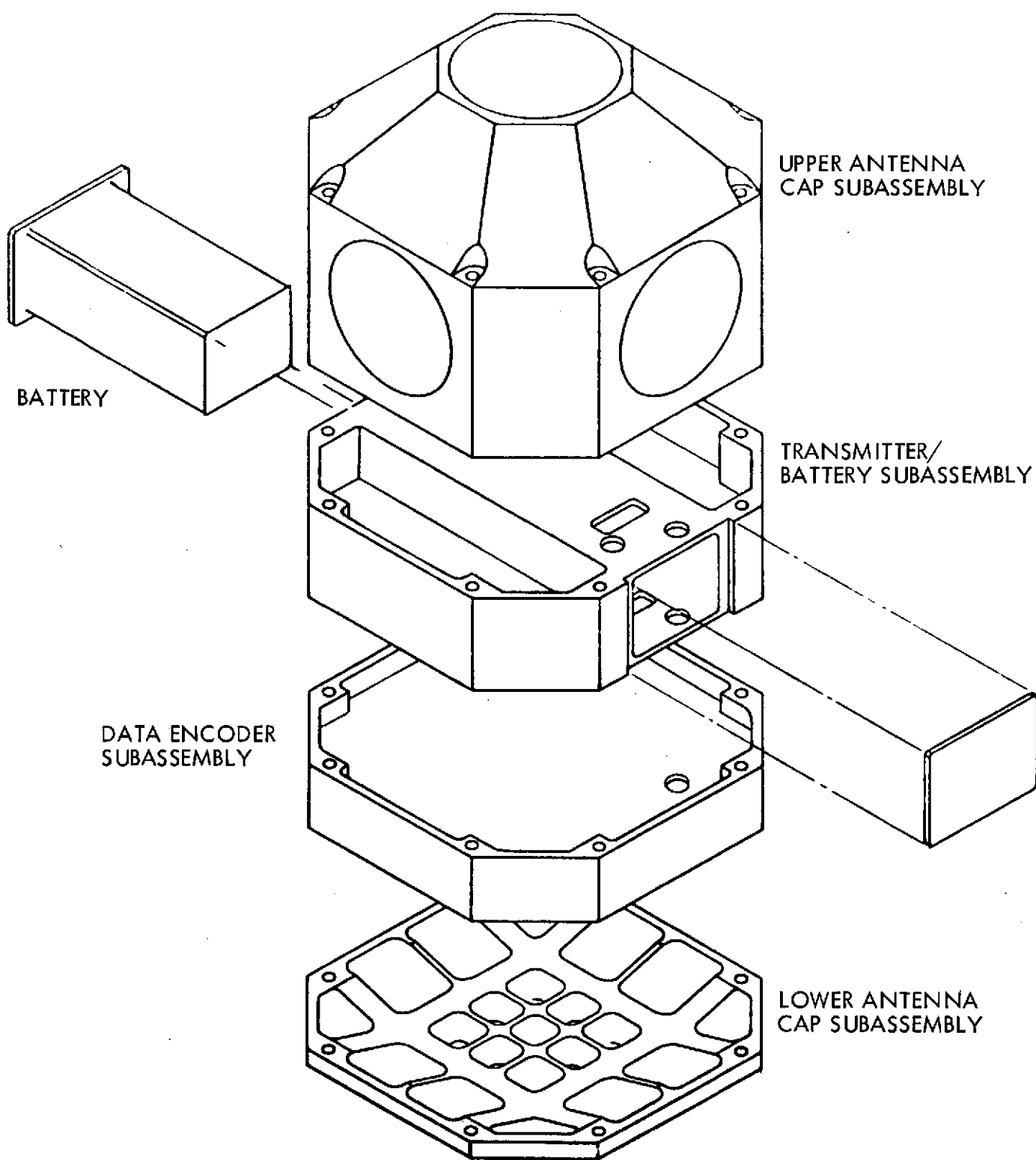


Fig. 5. CDR subassembly

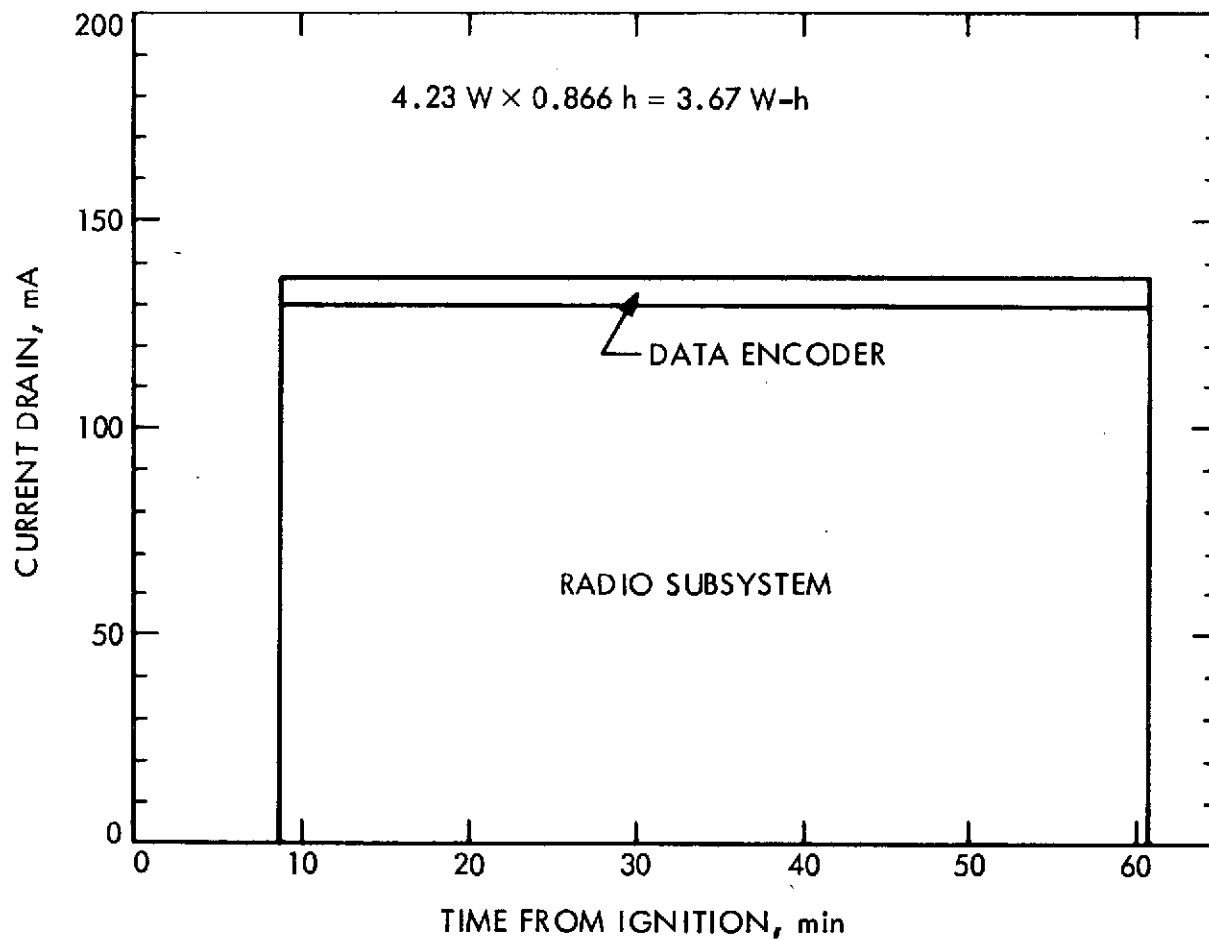


Fig. 6. CDR battery I (28 Vdc \pm 10%) current profile

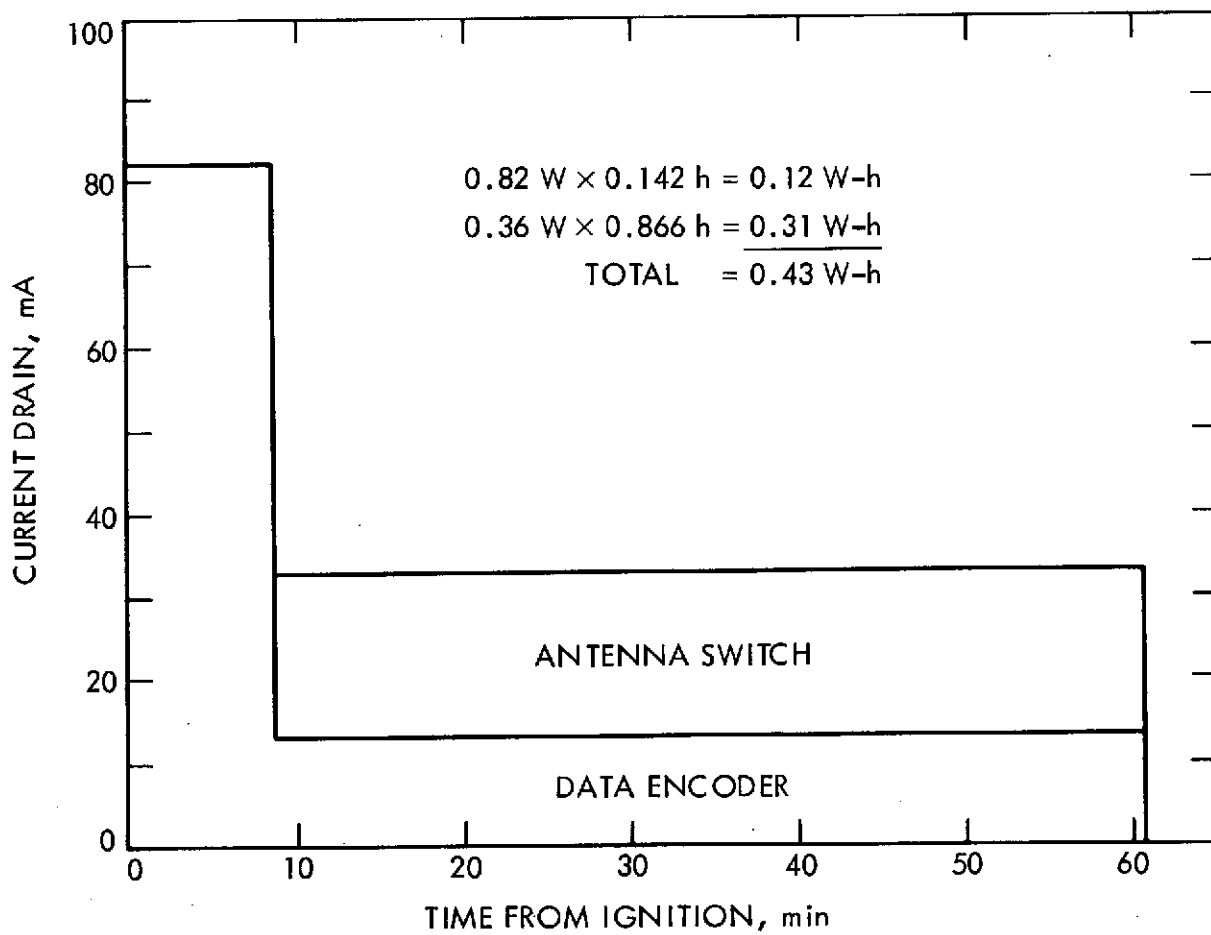


Fig. 7. CDR battery II (10 Vdc \pm 10%) current profile

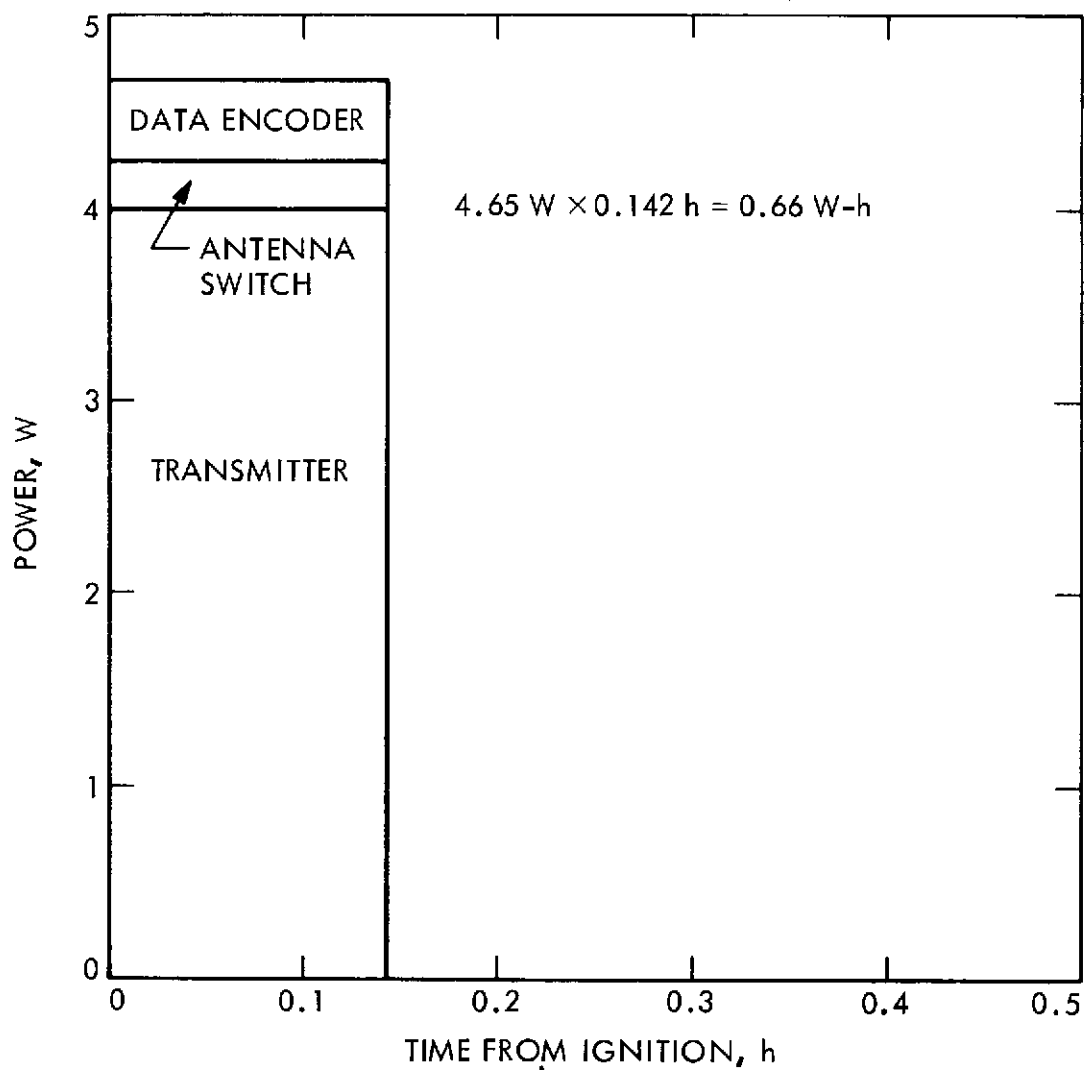


Fig. 8. CDR power for real-time data mode

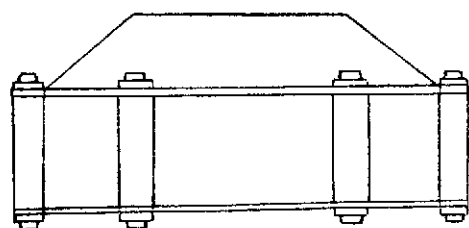
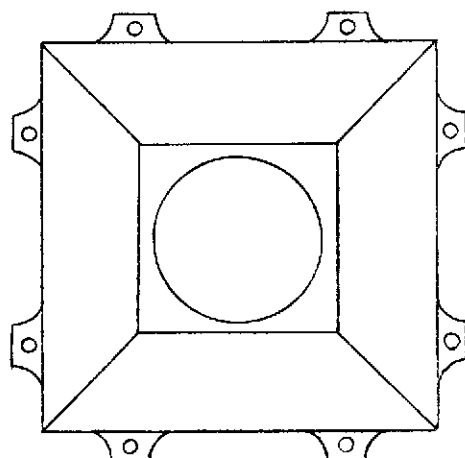


Fig. 9. Unhardened CDR
design subassembly

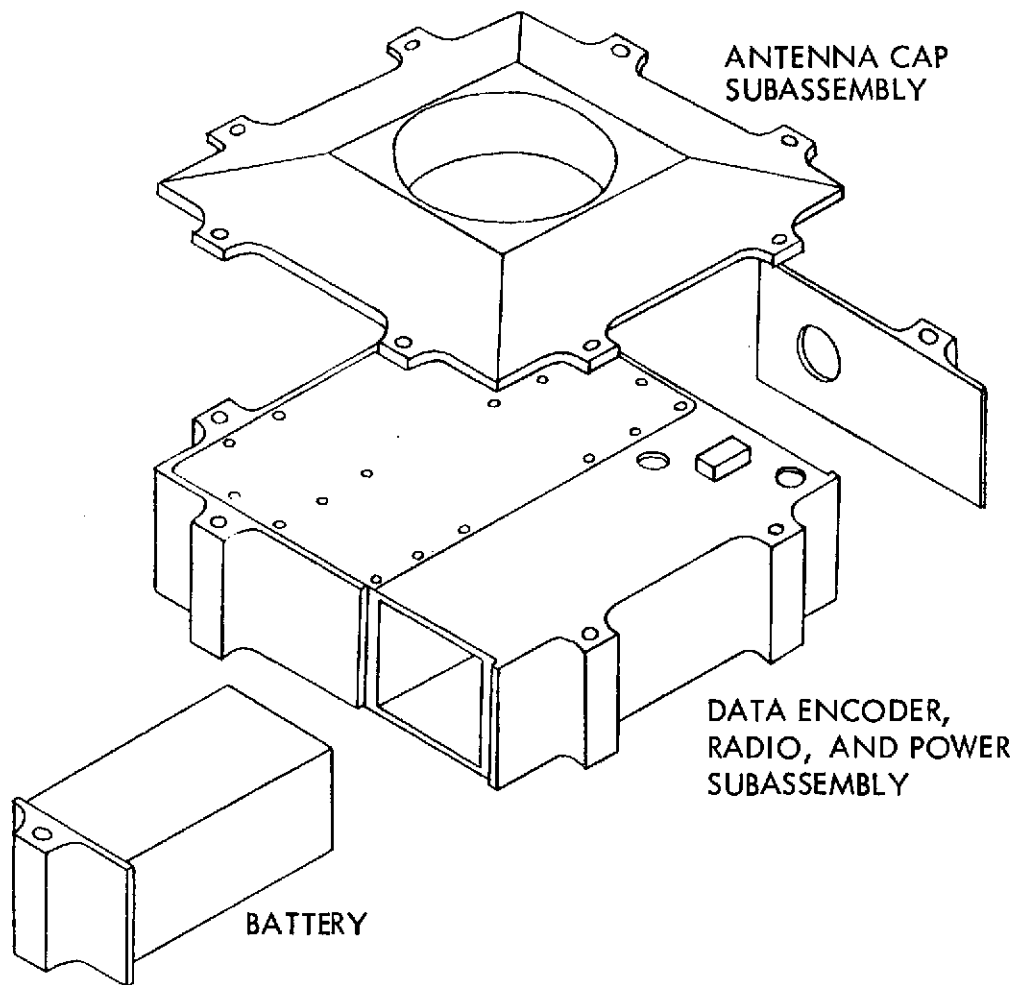


Fig. 10. CDR subassembly integration—unhardened design

APPENDIX

TYPICAL SOLID MOTOR SPECIFICATION REQUIREMENTS

Table A-1. SVM-1 specification requirements

Total impulse	19 km s ⁻¹ to 158 kg payload (5800 ft/s to 349 lb payload)
Thrust	15,600 N at 278 to 311 K (3500 lbf at 40 to 100° F) 16 g (vacuum at 311 K) (16 g [vacuum at 100° F])
Chamber pressure	3.31 × 10 ⁶ Pa (480 psia)
Spin condition	69.4 ± 13.9 rad s ⁻¹ (125 ± 25 rpm)
Load factors	1.4 MEOP ^a (burst strength) MEOP = 3.31 × 10 ⁶ Pa (480 psia)
Time in space	48-h min.
Case temperature (maximum permitted during burn)	589 K (600° F)
Service temperature	278 to 311 K (40 to 100° F)
Acceleration	
Thrust	24 g, 10 min
Lateral	3 g, 10 min
Rotation	35 rad s ⁻¹
Storage time	1 yr min.
Storage temperature	
Upper and lower limit	272 to 317 K (30 to 110° F)
Storage	297 ± 2.78 K (75 ± 5° F)
Transportation	294 ± 5.56 K (70 ± 10° F)
Storage humidity	
During transportation	< 50%
During storage	< 65%
Transportation mechanical shock	< 3 g
Transportation vibration	Not specified

^aMaximum equivalent operating pressure

Table A-2. SVM-2 specification requirements

Total impulse	20.9 km s ⁻¹ to 113-kg payload (6370 ft/s to 250-lb payload)
Thrust	13 g to spacecraft at 0 Pa (0 psia), 272 to 306 K (30 to 90° F)
Chamber pressure	3.64 × 10 ⁶ Pa (528 psia)
Spin condition	9.42 to 11.5 rad s ⁻¹ (90 to 110 rpm)
Load factor	1.4 MEOP ^a (burst strength) MEOP = 3.64 × 10 ⁶ Pa (528 psia)
Time in space	10 days min.
Case temperature	Not specified
Service temperature	272 to 306 K (30 to 90° F)
Acceleration	
Thrust	14-g boost, 13 g at 11.5 rad s ⁻¹ (110 rpm) burn
Lateral	2-g boost
Storage time	3 yr min.
Storage temperature	267 to 322 K (20 to 120° F) at 65% humidity
Storage humidity	98% at 306 K (90° F) for 120 h
Transportation mechanical shock	Drop of 6.5 m (20 ft) to steel- faced concrete in shipping container
Transportation vibration	Not specified
^a Maximum equivalent operating pressure	

Table A-3. TE-M-521 specification requirements

Total impulse	3.19×10^{-5} N-s at 286 K (71,620 lbf-s at 55°F)
Thrust	2.22×10^4 N (5000 lbf) max (vacuum) [(9.34×10^5 N s ⁻¹ max rise) (210,000 lbf/s max rise)]
Spin condition	10.5 rad s ⁻¹ (100 rpm)
Load factors	1.25 MEOP ^a
Time in space	Not specified
Case temperature	700 K (800°F)
Service temperature	256 to 317 K (0 to 110°F)
Acceleration	
Longitudinal	15-g launch 25-g burn
Lateral	2-g launch 1-g burn
Storage time	2 yr minimum
Storage temperature	256 to 317 K (0 to 110°F) [(244 and 339 K for 8 h) (-20°F and 150°F for 8 h)]
Storage humidity	100% with condensation (no time stated)
Transportation mechanical shock	With motor in shipping container: (a) half sine, 15-g peak, 11 ms, 3 per direction and (b) using one end as pivot, other end is lifted 10.2 cm and dropped to wooden benchtop, 4 per face
Transportation vibration	Not stated

^aMaximum equivalent operating pressure

Table A-4. TE-M-364-3 specification requirements

Total impulse	1.86×10^6 N-s at 306 K (418,400 lbf-s at 90°F)
Thrust	5.34×10^4 N (12,000 lbf) at 306 K (90°F) for 43 s
Spin condition	11.5 rad s^{-1} (110 rpm)
Load factors	1.5 MEOP at 306 K (90°F) (burst pressure)
Time in space	66 h min.
Case temperature	783 K (950°F)
Service temperature	289 to 306 K (60 to 90°F)
Acceleration	
Ignition	10 g
During burn	30 g
Storage time	2-yr min.
Storage temperature	278 to 311 K (40 to 100°F)
Storage humidity	< 50%; 95% at 311 K (100°F) for 42 h
Transportation mechanical shock	With motor in shipping container and supporting one end 15.2 cm (6 in.) above ground, other end is dropped from height of 61 cm (24 in.) to concrete, 1 per edge
Transportation vibration	1.3 g; 2.54 cm (1 in.) double amplitude displacement 1 to 5 Hz; roll off double-amplitude displacement from 2.54 cm (1 in.) to 0.091 cm (0.036 in.) from 5 to 26 Hz; 0.091 cm (0.036 in.) double-amplitude displacement from 26 to 52 Hz

Table A-5. FW-4S specification requirements

Total impulse	7.65×10^5 N-s (172,042 lbf-s)
Thrust	2.38×10^4 N (5349 lbf) (average)
Chamber pressure	4.16×10^6 to 5.29×10^6 Pa at 278 to 311 K (604 to 767 psia at 40 to 100° F)
Spin condition	20.9 rad s^{-1} (200 rpm)
Load factors	$1.3 \times$ limit loads
Time in space	Not specified
Case temperature	533 K (500° F)
Service temperature	278 to 311 K (40 to 100° F)
Acceleration	14 g thrust plus 3 g lateral at 325 K (125° F) 18 g thrust plus 20.9 rad s^{-1} (200 rpm)
Storage time	1-yr min.
Storage temperature	272 to 317 K (30 to 110° F)
Storage humidity	Not specified
Transportation mechanical shock	Not specified
Transportation vibration	Not specified

Table A-6. TE-364-1 specification requirements

Total impulse	1.67×10^6 N-s (376,000 lbf-s) $\pm 1\%$
Thrust	4.45×10^4 N (10,000 lbf) max
Chamber pressure	4.03×10^6 Pa (585 psia) max
Spin condition	3-Axis stabilized
Load factors	1.1 MEOP ^a (proof)
Time in space	72-h min. cislunar space
Case temperature	589 K (600°F) max
Service temperature	267 to 317 K (20 to 110°F)
Acceleration	
Axial	9.1 g
Lateral	4.0 g
Storage time	1 yr
Storage temperature	267 to 311 K (20 to 100°F)
Storage humidity	3 to 95% RH
Transportation mechanical shock	Two 45.7-cm (18-in.) vertical drop tests in the shipping container onto concrete pad (nozzle up)
Transportation vibration	Not specified

^aMaximum equivalent operating pressure
